

POLITECNICO DI TORINO

Corso di Laurea Magistrale in
Ingegneria Meccanica

Tesi di Laurea Magistrale

Numerical model of a balloon-based
cryogenic probe



Relatore

Prof. Claudio Dongiovanni

Candidato

Nicholas Scialanca

Abstract

Atrial fibrillation is a disease that alters the speed and rhythm of the heart-beat, greatly affecting the patient's quality of life. To treat recurrent forms, the pulmonary veins are electrically isolated, freezing the cardiac tissue surrounding them. This treatment is carried out using a cardiac probe consisting of a capillary for the delivery of the coolant in a inflatable expansion chamber, and a return line to discharge the exhausted fluid.

The aim of this thesis is to develop a 1-D numerical model of a balloon-based cryogenic probe. The behaviour of the fluid inside the injection and return line was modelled writing the continuity, momentum and energy equations under steady-state assumption, and implementing a homogeneous model for two-phase fluid.

The fluid friction was evaluated using an empirical correlation. In order to select the most suitable model for the case under consideration, a comparison of the various available ones was carried out.

In order to direct the fluid towards the walls of the balloon, small orifices are present at the end of the capillary, for this reason a flow model was implemented in order to preliminarily assess the mass flow rate disposed of by the probe.

Single-phase and two-phase heat transfer models were also introduced in order to simulate the heat exchanged by the lines.

The system of ordinary differential equations was discretized using the finite volume approach, and the resulting system of non-linear equations was solved using the iterative Newton-Raphson procedure.

The developed numerical model was experimentally validated by means of a tailor-made test bench.

Finally, the performance of a commercial cryoballoon was simulated and the numerical results obtained were compared with those available in the literature.

Contents

List of Figures	3
List of Tables	5
1 Introduction	6
1.1 Atrial fibrillation	7
1.2 Cryoablation	9
2 Cardiac cryoablation catheter description	13
2.1 Connection line	14
2.2 Injection holes	15
2.3 Expansion chamber	15
3 Mathematical model	17
3.1 Two-phase gas-liquid flow models	18
3.2 Governing equations	19
3.3 Flow rate model	22
3.4 Balloon energy conservation	25
4 Phenomenological correlations	27
4.1 Friction models	27
4.2 Dynamic viscosity models	29
4.3 Heat transfer correlations	30
4.3.1 Single-phase	31
4.3.2 Two-phase	33
5 Solving method	35
6 Comparison of friction and dynamic viscosity models	39
7 Experimental Setup	44
8 Results and Discussion	48

9 Performances of a commercial probe	58
10 Conclusions	66

List of Figures

1.1	Schematic drawing showing catheter ablation of AF using either RFA or CA with a balloon-based tip [6].	8
1.2	Cryoconsole system connected to Arctic Front Advance Cardiac or Freezor Cryocatheter Ablation www.medtronicacademy.com	10
1.3	Internal details of CP line.	11
1.4	A: Diagram of the inner components of a tip-based cryo-catheter (from Medtronic) [37]. B: Arctic Front Advance PRO catheter cryoballoon inner components www.medtronicacademy.com	12
2.1	Schematic representation of connection line and balloon.	13
2.2	Schematic view of the return and injection line arrangement.	14
2.3	Image of the coiled capillary of the Arctic Front obtained through Computed Axial Tomography probe and detail of an hole obtained using a Scanning Electron Microscope.	15
3.1	Flow patterns in horizontal channel [15].	18
3.2	Representations of 3 isentropic expansions in a p-h graph with $p_i = 32\text{bar}$ and $h_A = 100\text{J/g}$, $h_B = 200\text{J/g}$, $h_C = 550\text{J/g}$	23
3.3	Development of the normalized mass flow rate for the 3 initial conditions in Figure 3.2 as a function of the expansion ratio.	24
3.4	Specific mass flow trends as a function of upstream conditions ($p^o h^o$), in detail the points corresponding to the transformations in Figure 3.2.	25
3.5	Schematic view of the balloon.	26
4.1	Trend of friction coefficient as a function of Reynolds number for $\epsilon/D = 3.5 \cdot 10^{-3}$ with different correlations.	27
4.2	Trend of dynamic viscosity models for N2O at p=30 bar.	29
5.1	Trends of length Δx as a function of position, when parameter k varies fo L=3.5 m e N=100.	35
6.1	Schematic representation of the capillary.	39

6.2	Comparison of experimental simulated pressure trends for the conditions described in table 6.1 from A to D	42
6.3	Comparison of experimental simulated pressure trends for the condition described in table 6.1 case E	43
7.1	Schematic representation of the experimental setup.	44
7.2	Simulation results: $p_0=30$ bar, $T_0=18$ °C $G=204$ mg/s $T_{cold}=-25$ C° $L_{HE}=4$ m.	45
7.3	Simulation results with the last meter that exchanges in the air : $p_0=30$ bar, $T_0=18$ °C $G=204$ mg/s $T_{cold}=-50$ C° $L_{HE}=6$ m	47
8.1	Comparison of measured vs simulated mass flow rate	49
8.2	a) : Experimental $T_{cold}=18$ °C. [b-c-d-e]: Capillary simulation with input value, experimentale temperatures and mass flow rate obtained from a) averaging in the last 100s ($p_0=23.7$ bar, $T_0=18.5$ °C and $G=81.9$ mg/s).	50
8.3	a) : Experimental $T_{cold}=-30$ °C. [b-c-d-e]: Capillary simulation with input value, experimental temperatures and mass flow rate obtained from a) averaging in the last 100s ($p_0=25.1$ bar, $T_0=-15$ °C and $G=100$ mg/s).	52
8.4	a) : Experimental $T_{cold}=-30$ °C. [b-c-d-e]: Capillary simulation with input value, experimental temperatures and mass flow rate obtained from a) averaging in the last 100s ($p_0=25.3$ bar, $T_0=-39.7$ °C and $G=377.0$ mg/s).	54
8.5	(High) Trend of measurements taken during the oscillatory phenomenon. (Low) Trend of measurements taken during the hole-clogging phenomenon.	55
8.6	A : experimental expansion chamber filled with liquid N_2O at ambient pressure and saturation temperature. B :the liquid start to freeze for the effect of a sudden reduction of pressure due to the connection of a vacuum pump.	57
9.1	(left) Inflation phase obtained with inlet pressure reduction while keeping the subcooling ($T_0=-25$ °C $p_0=12$ bar). (right) Inflation phase with subcooling bypass ($p_0=34$ bar $T_0=18$ °C).	59
9.2	(left) Adiabatic case with $N_{holes}=4$ ($T_0=-25$ °C $p_0=34$). (right) Diabatic case with $N_{holes}=4$ ($p_0=34$ bar $T_0=-25$ °C).	61
9.3	(left) Reduction in global heat exchange coefficient ($T_0=-25$ °C $p_0=34$ bar $k_B=300$ $W/(m^2K)$). (right) Increase in global heat exchange coefficient ($T_0=-25$ °C $p_0=34$ bar $k_B=500$ $W/(m^2K)$).	64

List of Tables

6.1	Input data for the simulation [40].	40
6.2	Results comparison between experimental and simulated values. . .	41
9.1	Effect of varying the number of holes (adiabatic lines) for inlet condition $T_0=-25^\circ\text{C}$ $p_0=34$ bar (Ablation phase).	62
9.2	Effect of varying the number of holes (diabatic lines) for inlet condition $T_0=-25^\circ\text{C}$ $p_0=34$ bar (Ablation phase).	63

Chapter 1

Introduction

The fight against death in which the human race took part around 300 000 years ago is far from being won. Since the dawn of species, methods have been sought (albeit often ineffective) to cure disease and prolong life.

Since Hippocrates, who took Greek medicine out of its pre-scientific phase, linked to magic and religion, and organised it with a rational, rigorous and empirical methodology, scientific development has made great strides, but death and many illnesses are a limit that has not yet been overcome.

Study of death has interested countless people throughout history, but for now it is physically impossible to avoid it, the human being, like every object known to man, comes up against the passage of time, the wearing down of his body. Human race has regeneration processes to deal with this problem, but they are not unlimited and infinite, just as an object at a certain point can no longer be fixed, so for now the human being is destined to die.

This fear of inevitable "darkness" has led human beings to strive for a state of immortality, paying particular attention to the preservation of two elements that have always been considered fundamental: heart and brain.

The attention that man has devoted to his body has coincided with his self-awareness, identifying the heart as the container for emotions and the engine of that machine which allowed him to inhabit the world.

Essential and very vulnerable, this is why medicine has paid much attention to the study of this organ, with the aim of finding a way to limit natural erosion and cures for diseases that impair its functioning.

A disease in particular has become one of the most important public health issues, atrial fibrillation, the most common cardiac arrhythmia, with an estimated 2-3% of the population in Europe and North America affected in 2014[50], 33 million worldwide in 2020[12], and is expected an increase in cases over time due to

the rise of average life expectancy and by the increasing incidence and prevalence of risk factors like obesity, physical inactivity, sleep apnea, diabetes mellitus, hypertension, and other modifiable lifestyle-related factors.

To tackle this disease, a new technology has joined the existing ones, cryoablation via balloon catheter, developed in parallel by two companies, Boston Scientific and Medtronic.

1.1 Atrial fibrillation

Atrial Fibrillation (AF) is a heart rhythm abnormality characterised by irregular and rapid beats of the atrial chambers due to the production of electrical impulses originating from atrial myocytes ¹, although it is not a life-threatening disease, it greatly affects the patient's quality of life, increases the risk of heart failure, dementia and ischaemic stroke, and also causes severe socio-economic problems such as permanent disability, cognitive impairment, frequent hospitalization and absence from work.

Given the nature of this disease, it is normally treated with two different objectives:

- **Rate control:** slowing down the heart rate to bring it closer to a normal range;
- **Rhythm control:** changing the rhythm to a normal sinus one.

In both cases, targeted pharmacological therapy is mainly used, but in cases of chronic or reoccurring AF in selected patients, where sinus rhythm cannot be maintained over time, ablation is used.

The aim of an ablation-based technique is to inhibit by destroying defective cardiomyocytes in specific parts of the atria, to restore the normal rhythm. From the study of 45 patients with frequent cases of drug-resistant AF, it was identified that out of 69 points of origin, 94% of them were located around the Pulmonary Veins (PVs) [25], this discovery led to the development of Circumferential Pulmonary Vein Isolation (CPVI) [2], where the cardiac tissue surrounding the PV is ablated.

The most commonly used ablation method at present is Radiofrequency Ablation (RFA), where the connective tissue of the heart is damaged by heat generated from medium frequency alternating current. However, considering that the diameter of a pulmonary valve ostium varies in a range from 7 to 27 mm (depending on

¹ muscle cells that compose the cardiac muscle

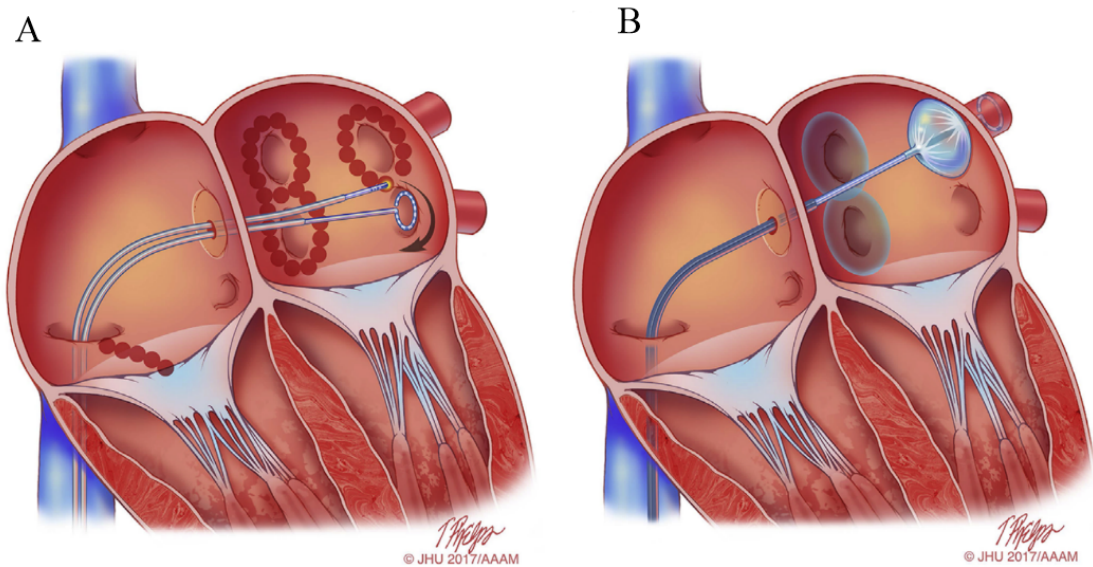


Figure 1.1. Schematic drawing showing catheter ablation of AF using either RFA or CA with a balloon-based tip [6].

the position inside the left atrium) [48], and the catheter tip is a few millimetres in diameter (for example the one used in [39] is around 3 mm), as can be seen from Figure 1.1.A, multiple applications are required in order to obtain a continuous circumferential lesion.

Moreover, although it is the most widely used method in the world, the percentage of patients in which atrial arrhythmia no longer recurs is not satisfactory [9]. Alternative methods are emerging, such as :

- **Cryoablation:** a process that aims at tissue damage by inducing cell freezing;
- **Laser ablative therapy:** tissue is damaged by the absorption of energy by intracellular and extracellular water, transformed in heat;
- **Ultrasound ablation:** tissue are damaged by the heating produced by absorption of the ultrasonic energy and tissue cavitation.

Particular attention should be paid to Cryoablation, which, as will be explained in the next section, is becoming increasingly popular thanks to the development of Cryoballoon (CB), which allows PV to be isolated with a single application like in Figure 1.1.B.

1.2 Cryoablation

Since ancient times, the usefulness of cold in treating wounds, infections or ulcers was well known. Interest in these effects led to the emergence of cryosurgery between 1845 and 1851, when James Arnott (1797-1883) described the benefits of using a salt ice solution (about -20°C) to treat certain types of cancer[21], while cardiac cryoablation was introduced by Hass and Taylor[26] in the period of 1947 and 1951, as an alternative method to radiofrequency ablation.

CA involves extracting heat from the tissue, causing hypothermia and consequently loss of cells function. These effects can be temporary or permanent, depending on the temperature and duration of the process. If target is brought into a temperature range between 0 and -5°C , its functions can be restored simply by letting it thaw, whereas at a temperature of around -20°C held for more than 4 minutes or at a temperature below -50°C regardless of time, the cells are permanently damaged [37]. Cryomapping is based on this property, as it is possible to study the effect of freezing on electrically active tissue, controlling any undesirable reactions without permanently damaging the cells [49] [7].

CA procedure is performed by means of a catheter (cryoprobe). The first was invented in 1961 by Cooper and Lee[16], consisted of a vacuum-isolated tube which transports liquid nitrogen to the tip where it is vaporised, leading to heat absorption from the adjacent tissue, the resulting gas is then disposed of and a thermocouple placed in the tip allowed temperature to be controlled [5]. For cryosurgery it was a revolution, as it was an easily manoeuvrable and non-invasive tool.

Another property, in addition to the system described for the Cooper and Lee probe, is used to cool the fluid to the operating temperature, the Joule-Thomson Effect, a phenomenon whereby the temperature of a real gas or liquid changes when it is forced through a valve or an hole without heat exchange with the environment, in this specific case it expands isentropically reducing its temperature.

In addition, in the case of a fluid that from a liquid state reaches saturation temperature during heat exchange, the latent heat of evaporation is used to absorb more heat from the system.

The most commonly used refrigerants are nitrous oxide (N_2O), argon (Ar) and nitrogen (N_2), each of these fluids have different cryosurgery temperatures and types of use.

The Figure 1.2, shows a classic CA system, as can be seen, is present the cryoconsole, which is connected to a catheter via an electrical cable and a coaxial tube for liquid gas line, at the end of the catheter there is the tip, the element that actively produces tissue freezing, which depends on the cryoprobe type.

The cryoconsole represents the management system for the CA procedure, its

functions are:

- house the refrigerant;
- pre-cooling of refrigerant
- monitor temperature and pressure during the process;
- regulate the flow rate of refrigerant to be delivered into catheter;
- create a vacuum for the return of gas from catheter;
- dispose of the exhausted gas.

The cable and the tube represent the connection line, one contains the electrical connections necessary to transfer information from the sensors in the tip to the Cryoconsole interface, while the other the refrigerant injection and return lines. As can be seen in Figure 1.2 and in more detail in Figure 1.3, the two separate sections of the connection line converge within a steerable sheath, forming, with the deflection wires, the cryoprobe line.

The catheter ends with the tip, which differs from model to model, the elements commonly found inside, in addition to those already seen in the CP line, are the thermocouple to control the temperature in the tissue in contact, sensors for the electrocardiogram and the expansion chamber, where the refrigerant is forced

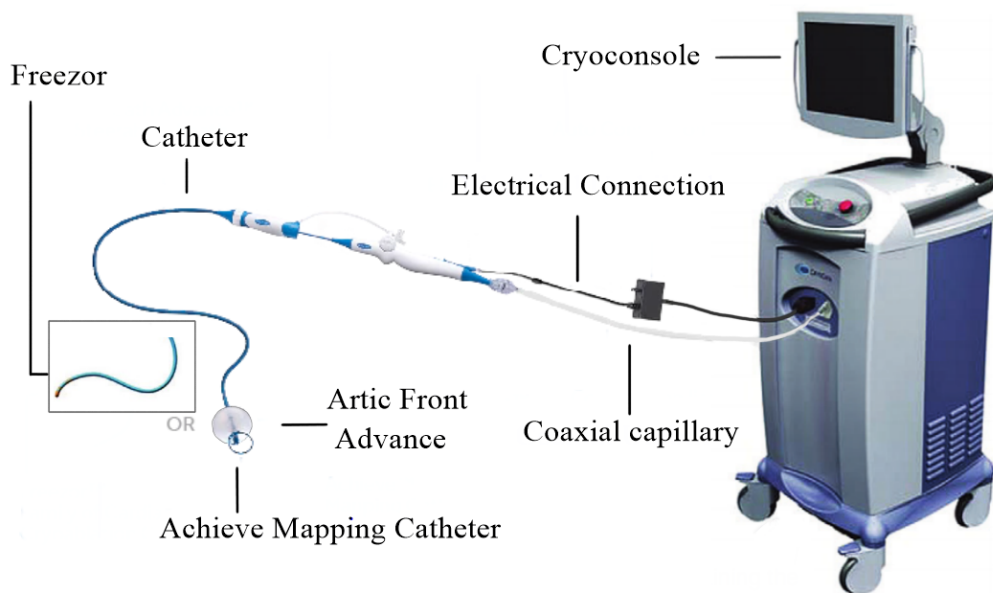


Figure 1.2. Cryoconsole system connected to Arctic Front Advance Cardiac or Freezor Cryocatheter Ablation www.medtronicacademy.com.

through to expand, so that the tip temperature is reduced in order to proceed with the CA.

Regarding pulmonary vein (PV) ablation two types of catheter are currently used: tip ablation and balloon-based.

Both types use JTE to cool the tip. The first consists of a conductive tip with a diameter of a few millimetres (3 mm in diameter, taking into account Medtronic's Frezor Max) like the one shown in Figure 1.4.A. Similar to using the RFA, due to its relatively small size, several applications are required to ablate the entire area needed to restore normal atrial rhythm, as a result, therapy takes a long time and success depends very much on the skill of the therapist.

To overcome these problems, a balloon-based tip was developed, in order to have a larger contact area (balloon diameter from 23 to 28 mm) which allows ablation to be carried out in a single application, but without the need for a more intrusive catheter, as the balloon is guided deflated into the cardiac atrium and inflated to the desired position. As can be seen from Figure 1.4.B components of the CB are the same as before, but the expansion chamber is made up of dual polymeric balloons, the liquid is vaporised and directed towards the surface of the inner balloon through holes slightly distant from the equator (4 holes for Medtronic's Artic Front or 8 holes for Medtronic's Artic Front Advance).

Aware of the relevance of a device that can reduce the incidence of a disease that will place an increasing burden on society and the national health system, this work focuses on creating a tool that can provide an help in analysing and understanding the mechanisms that take place within this probe. Using the Artic Front family of cryoprobes (Medtronic, Inc., Minneapolis, MN) as a starting point, the aim was to create a mathematical model to derive the behaviour of the cryogenic fluid, for any design and off-design conditions of the CP.

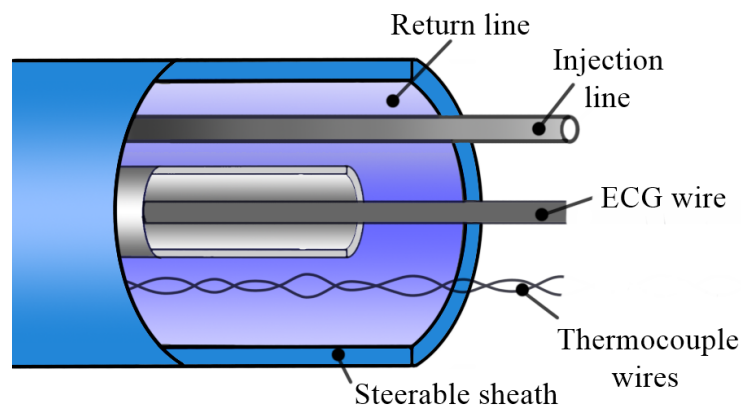


Figure 1.3. Internal details of CP line.

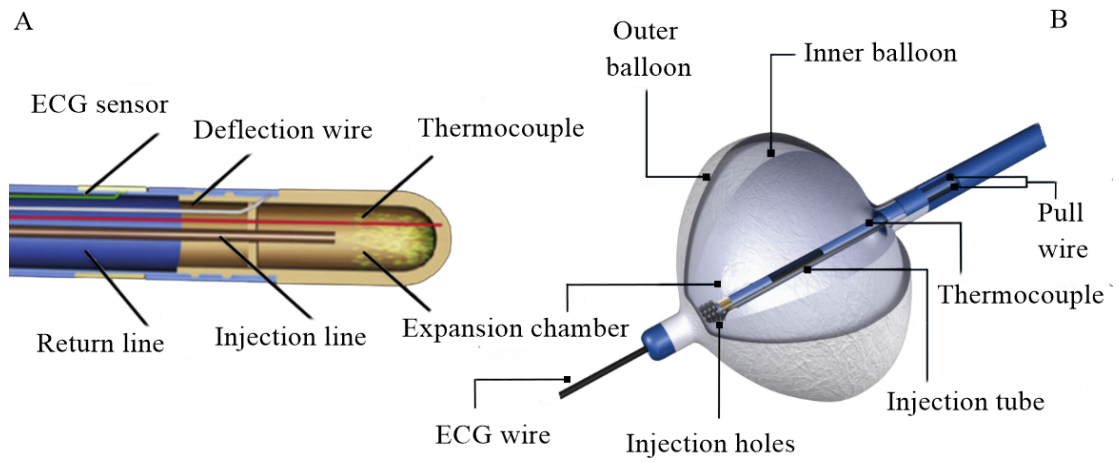


Figure 1.4. **A:** Diagram of the inner components of a tip-based cryo-catheter (from Medtronic) [37]. **B:** Arctic Front Advance PRO catheter cryoballoon inner components www.medtronicacademy.com

Chapter 2

Cardiac cryoablation catheter description

The starting point of the work is the definition of the system to be modelled, actually only two companies produce models of a balloon-based cryoprobe, Medtronic and Boston Scientific. The choice fell on the Artic Front family of probes developed by Medtronic, as unlike other competing companies, they have been much studied and many references and data can be found in literature.

Once the probe has been selected, it is possible to move on a detailed description of the elements that make it up. The main components are: connection line and expansion chamber.

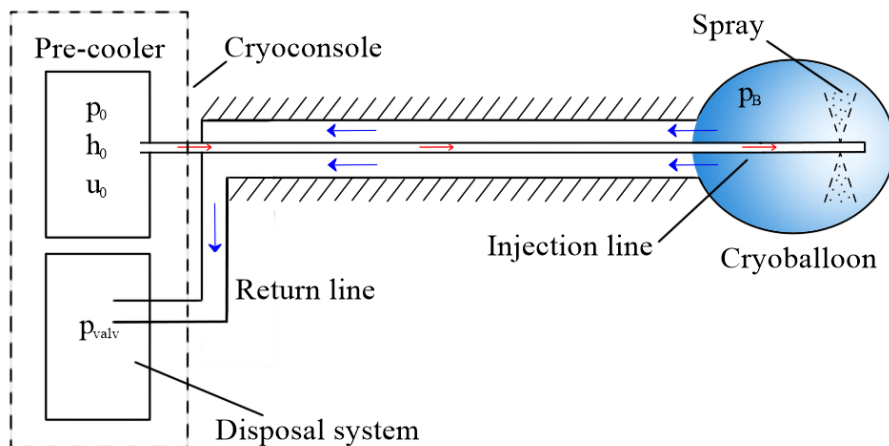


Figure 2.1. Schematic representation of connection line and balloon.

2.1 Connection line

From now on, the connection line will be understood as the pipe connecting the Cryoconsole to the tip, where, as can be seen from Figure 2.1, the Injection Line (IL) and Return Line (RL) can be identified inside, disregarding the electrical and mechanical elements.

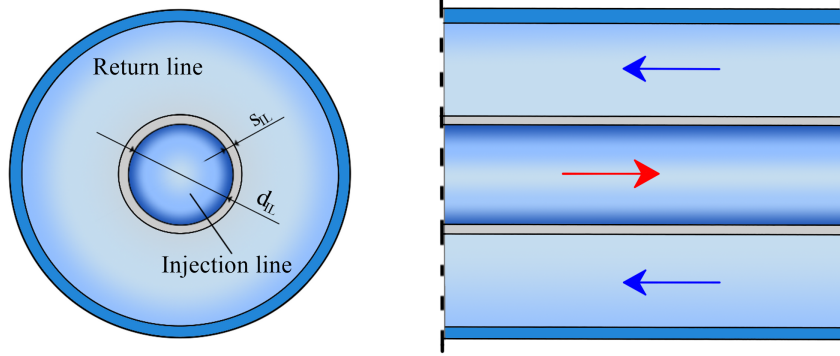


Figure 2.2. Schematic view of the return and injection line arrangement.

Connection line consists of a 3.5 m catheter, the outer surface is a directional plastic sheath, considering the material and the thickness of 0.3 mm, it is assumed that heat exchange to the outside is negligible. As mentioned, the interior consists of the two transport lines, which for simplicity are considered coaxial as in Figure 2.2, the IL with an inner diameter of 0.31 mm ($d_{i,IL}$) and a thickness of 0.078 mm (s_{IL}) that guides the fluid to the expansion chamber, surrounded by the RL, which given the complexity of the geometry has been assumed to be an annular with a hydraulic diameter of 1.0 mm ($d_{h,RL}$), which on the other hand, transports the exhausted fluid from the balloon to the cryoconsole disposal system. In order to match the RL pressure drop estimated from literature [17], assuming the mass flow rate [47] during ablation phase, the hydraulic diameter was obtained .

To determine the effect of the friction on the pressure drop and consequently on the fluid property, it is essential to define the roughness(ϵ). It was not possible to carry out specific measurements, however capillary roughness is estimated from literature ([28] [34]) to be in the range of 3.0-0.6 μm . In spite of the different material of the return line, given the preliminary nature of this thesis work, the same roughness value corresponding to $\epsilon=1.0 \mu\text{m}$ was chosen for both lines.

2.2 Injection holes

The IL ends with a holed helical structure like the one in Figure 2.3 that through orifices with a diameter of $62\ \mu\text{m}$ releases the fluid inside the CB. The holes direct the coolant towards the walls of the expansion chamber that will be in contact with the area to be ablated.

Coiled capillary leads to an increase in pressure drop compared to a straight one [38]. Given the shortness of the helical section compared to the whole capillary, the effect on the flow is negligible. Accordingly injection line is considered as completely straight capillary.

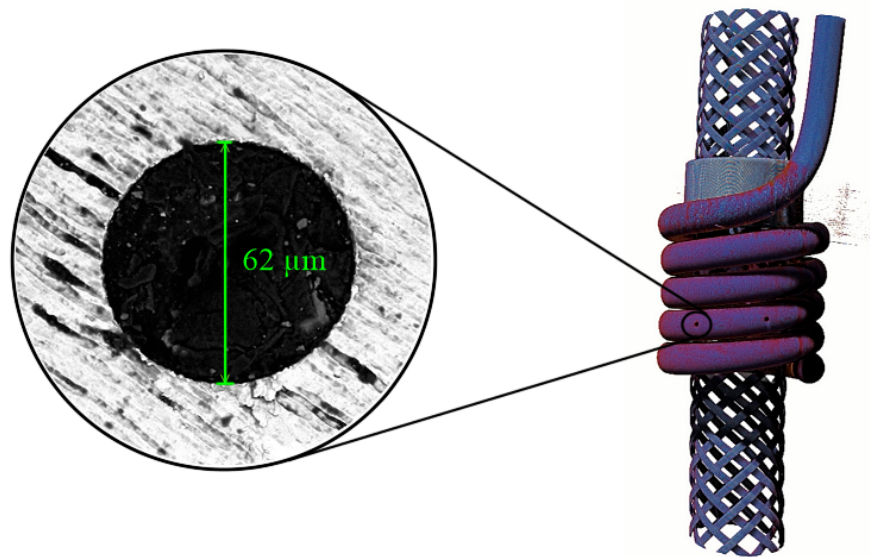


Figure 2.3. Image of the coiled capillary of the Artic Front obtained through Computed Axial Tomography probe and detail of an hole obtained using a Scanning Electron Microscope.

2.3 Expansion chamber

The expansion chamber consists a balloon made of two layer of polymeric material, with a diameter of $d_B = 28\ \text{mm}$. Once positioned, the balloon exchanges heat with the human tissue to be ablated. To get an estimated value of the heat exchanged by the balloon, knowing that the total surface is assumed to exchange with pulmonary vane surface and blood, a global heat transfer coefficient is used.

To perform the ablation, two stages are required, a first one of inflation, where

the balloon is fed by gas only, in order to inflate the expansion chamber. A second one of ablation, where the refrigerant is cooled and in liquid state sent to the injection line. Within the injection line, the liquid may expand to evaporation conditions. The fluid inside the probe can be found in gas-only, liquid only and two-phase.

Chapter 3

Mathematical model

As regards the elements of the connection, injection and return line, the fluid-dynamic and thermal behaviour of a fluid flowing in a capillary has to be modelled.

The modelling of a cryogenic fluid flowing inside a microchannel is a problem that is widely addressed in the literature [22][27][11], since a capillary is normally used as an expansion device in refrigeration systems. From the literature cited above, it can be seen that a phase change has to be considered when studying the behaviour of a sub-cooled liquid forced to expand inside a capillary, consequently a two-phase fluid must also be taken into account.

Modelling can be done using different approach:

- **Empirical models**

based on empirical correlations between flow parameters and capillary geometry;

- **Lumped models**

an appropriate equivalent circuits is used to describe the fluid system, representing pressure as the voltage and flow as the current;

- **Distributed models**

based on solving the equations of conservation of mass, momentum and energy, applied to one-dimensional control volumes distributed along the domain following the discretization trend.

As there are no usable experimental data or equivalent circuits for the system under analysis, a distributed model was developed, so that the trends of the main fluid properties can be obtained.

3.1 Two-phase gas-liquid flow models

Considering a two-phase fluid, gas and liquid phases form peculiar patterns that affect properties such as pressure drop and heat transfer. The flow patterns types are influenced by thermodynamic and hydrodynamic equilibrium conditions. Those observable in a biphasic flow in horizontal tubular pipe are those shown in Figure 3.1[15]:

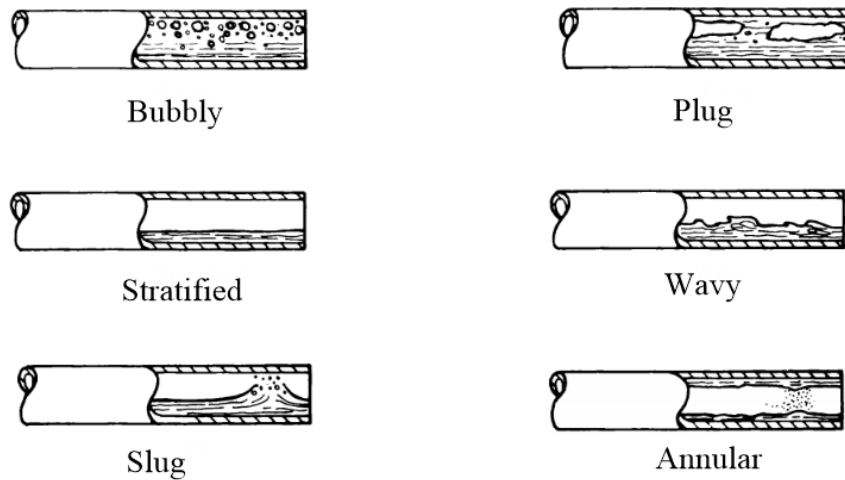


Figure 3.1. Flow patterns in horizontal channel [15].

Given the influence of the pattern in fluid properties, it is necessary a way to model a two-phase flow.

As described in [15] the main used are :

- **The "Homogeneous" flow model**

is the simplest approach, it is based on the assumption that the biphasic, should be treated as a mono-phasic fluid with equivalent fictitious properties, that are obtained by combining the properties of the individual phases in an appropriate way.

The main assumptions that must be made in order to use this method are:

- liquid and vapour phases have the same velocity;
- thermodynamic equilibrium exist between phases.

Although this method best approximates patterns like the bubbly or the wispy-annular flow, for its computational simplicity it is used indiscriminately for all types of flow [15].

- **The "Separated" flow model**

the two phases are considered completely separate, it is necessary to write two sets of governing equations, one for each phase, and to know the sliding relationship between them.

In this case, the assumptions are:

- liquid and vapour phase have different velocities;
- thermodynamic equilibrium exist between phases.

This method better approximates the annular flow pattern, but compared to the first method has a higher complexity[15].

The work of Motta, Parise, and Braga[35], experimentally classifies the flow pattern of a biphasic fluid within a capillary as a being of bubbly-type, for this reason the "Homogeneous" model was used in this thesis.

3.2 Governing equations

Following the homogeneous approach, it is necessary to write the conservation equations of mass, momentum and energy. Some assumptions are applied in order to obtain a set of equations valid for both the probe lines.

The following assumptions have been introduced:

- pipes are assumed to be straight;
- the probe axis is horizontal and coincide with x-axis;
- constant wall roughness, diameter and cross section over the length ;
- refrigerant is pure;
- axial heat transfer is neglected;
- the refrigerant behaves like a Newtonian fluid;
- properties of refrigerant are constant in a cross section;
- no heat sources are within the fluid;
- transient behaviour are neglected.

Starting from the assumption of zero velocity in y and z axis and horizontal pipe, the governing equations for the x-axis became:

$$\frac{\partial \rho}{\partial t} + \frac{\partial(\rho \cdot u)}{\partial x} = 0 \quad (3.1)$$

$$\frac{\partial(\rho \cdot u)}{\partial t} + \frac{\rho \cdot u^2}{\partial x} = -\frac{\partial p}{\partial x} + \frac{\partial \tau_{xx}}{\partial x} + \frac{\partial \tau_{yx}}{\partial y} + \frac{\partial \tau_{zx}}{\partial z} \quad (3.2)$$

$$\begin{aligned} \frac{\partial}{\partial t} \left[\rho \cdot \left(e + \frac{u^2}{2} \right) \right] + \frac{\partial}{\partial x} \left[\rho \cdot \left(e + \frac{u^2}{2} \right) \right] = \\ = -\frac{\partial(p \cdot u)}{\partial x} - \frac{\partial \dot{q}}{\partial x} + \frac{\partial(\tau_{xx} \cdot u)}{\partial x} + \frac{\partial(\tau_{yx} \cdot u)}{\partial y} + \frac{\partial(\tau_{zx} \cdot u)}{\partial z} \pm \dot{q}_w \end{aligned} \quad (3.3)$$

Where p is pressure, e energy, ρ density, u velocity, τ shear stress, \dot{q} internal heat source and \dot{q}_w is the heat exchanged for unit of length . For steady state and negligible internal heat source ($\frac{\partial \dot{q}}{\partial x}$):

$$\frac{\partial(\rho \cdot u)}{\partial x} = 0 \quad (3.4)$$

$$\frac{\partial(\rho \cdot u^2)}{\partial x} = -\frac{\partial p}{\partial x} + \frac{\partial \tau_{xx}}{\partial x} + \frac{\partial \tau_{yx}}{\partial y} + \frac{\partial \tau_{zx}}{\partial z} \quad (3.5)$$

$$\frac{\partial}{\partial x} \left[\rho \cdot \left(e + \frac{u^2}{2} \right) \right] = -\frac{\partial(p \cdot u)}{\partial x} + \frac{\partial(\tau_{xx} \cdot u)}{\partial x} + \frac{\partial(\tau_{yx} \cdot u)}{\partial y} + \frac{\partial(\tau_{zx} \cdot u)}{\partial z} \pm \dot{q}_w \quad (3.6)$$

The shear stress gradient can be replaced in eq.(3.5) by an empirical function f_w representing the wall friction. Neglecting the work of the viscous term and using the correlation between enthalpy(h) and inner energy $e = h - p/\rho$ in equation (3.6) the obtained equations are:

$$\frac{\partial(\rho \cdot u)}{\partial x} = 0 \quad (3.7)$$

$$\frac{\partial(\rho \cdot u^2)}{\partial x} = -\frac{\partial p}{\partial x} + f_w \quad (3.8)$$

$$\frac{\partial}{\partial x} \left[\rho \cdot u \left(h + \frac{u^2}{2} \right) \right] = \pm \dot{q}_w \quad (3.9)$$

A fourth "governing" equation has to be added, which, by means of the pressure and enthalpy values, gives the corresponding density value. In this work the role of the equation of state is played by *Refprop8*[29], represented by (f_s), which also provides average values of ρ during phase transitions.

$$\rho = f_s(p, h) \quad (3.10)$$

The governing equations are discretized using the finite volume method, where the domain is divided into many elementary volumes and the relationships between the neighbouring volumes are defined using the integral form of the equations defining the problem.

The integral form is obtained by integrating along x-direction the equations 3.7-3.8-3.9 and replacing the integral of f_w with an expression ($\overline{\Delta p_{f_w}}$) evaluated from empirical friction laws using average volume properties.

The resulting set of equations is:

$$\rho_{i+1} \cdot u_{i+1} - \rho_i \cdot u_i = 0 \quad (3.11)$$

$$\rho_{i+1} \cdot u_{i+1}^2 - \rho_i \cdot u_i^2 + p_{i+1} - p_i + \overline{\Delta p_{f_w}} = 0 \quad (3.12)$$

$$h_{i+1} + \frac{u_{i+1}^2}{2} - h_i - \frac{u_i^2}{2} \pm \frac{Q_{W,i}}{\rho_i \cdot u_i} = 0 \quad (3.13)$$

$$\rho_{i+1} - f_s(p_{i+1}, h_{i+1}) = 0 \quad (3.14)$$

In the above set of equation, some parameter has to be defined. Regarding 3.12, the unknown is $\overline{\Delta p_{f_w}}$ which is an experimental relationship that evaluates the pressure drop as a function of geometric and flow conditions:

$$\overline{\Delta p_{f_w}} = \bar{\lambda} \frac{\Delta x}{D} \bar{\rho} \frac{\bar{u}^2}{2} \quad (3.15)$$

\bar{u} and $\bar{\rho}$ are the average values within the control volume of velocity and density, Δx is the length of the volume, while $\bar{\lambda}$ is the average coefficient of friction which is obtained by means of empirical relations which will be described in the next chapter. The average value of a generic fluid property (y) of the i-th control volume si defined as the arithmetic mean between inlet and outlet conditions:

$$\bar{y} = \frac{1}{2}(y_{i+1} + y_i) \quad (3.16)$$

\dot{Q}_W is the heat exchanged in a generic volume through the pipe walls, the sign depends on the line being modelled, "+" for the capillary and "-" for the return line.

$$\dot{Q}_W = U \cdot \pi \cdot D \cdot \Delta x \cdot (T_{RL} - T_{cap}) \quad (3.17)$$

T_{RL} and T_{cap} are the temperatures of the fluid flowing in the return and injection line, D is mean diameter of the capillary. U represents the thermal transmittance, which depends on the geometry and type of heat transfer involved. This is defined as:

$$U = \left[\left(\frac{1}{\hat{h}_{IL}} \right) + \left(\frac{s_{IL} \cdot \ln(A_o/A_i)}{k_{steel} \cdot (A_o - A_i)} \right) + \left(\frac{A_i}{\hat{h}_{RL} \cdot A_o} \right) \right]^{-1} \quad (3.18)$$

where \hat{h} represents the convective heat transfer coefficient of the fluid involved, s_{IL} and k_{steel} are the thickness and the thermal conductivity of the capillary respectively, while A_i and A_o are the internal and external surface involved in the heat exchange. The convective heat transfer coefficient is defined as:

$$\hat{h} = \frac{Nu \cdot k_T}{D} \quad (3.19)$$

where Nu is the Nusselt number, which must be defined by experimental relations, k_T is the conductivity of the fluid.

For the complete representation of the probe, accessory equations are required to provide information on the disposable flow rate and the internal conditions of the balloon.

3.3 Flow rate model

The holes at the end of the injection line determine the flow rate disposed of by the probe. Taking advantage of the choked flow phenomenon, an equation providing this information will be added to the already mentioned set of equations.

Critical flows is encountered when a fluid from a high-pressure environment is brought into communication through a constriction with a receiver at a lower pressure. Critical conditions are reached when the velocities is no longer influenced by downstream conditions, a reduction in pressure no longer increases the flow rate.

The critical flow for gases is reached when the velocity of the fluid at the nozzle critical area increases to the sonicity ($Ma = 1$).

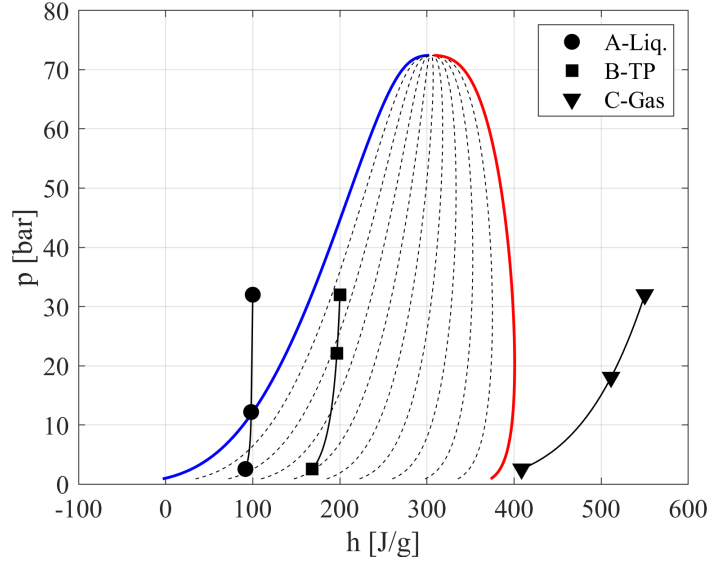


Figure 3.2. Representations of 3 isentropic expansions in a p-h graph with $p_i = 32\text{bar}$ and $h_A = 100\text{J/g}$, $h_B = 200\text{J/g}$, $h_C = 550\text{J/g}$.

In case of liquid, the phenomenon that limits the evolution of the velocity is different, critical condition is reached when the pressure drop due to the restriction brings the downstream pressure below the saturation one at the given temperature. At that point, the liquid partially flashes in vapour bubbles and their collapse causes cavitation. The critical flow is a very important parameter for determining the maximum flow rate of a system, assuming that it is necessary to simulate under all operating conditions, a two-phase model is also required.

The method implemented in this work, in accordance with the assumptions already made, is the Homogeneous Equilibrium Model (HEM). The basic assumptions to be met, in accordance to [18], are:

- homogeneity;
- thermodynamic equilibrium;
- isentropic and stationary flow.

Assumptions like homogeneity, thermal equilibrium and steady-state flow are at the basis of the method chosen for the simplification of the governing equations, to comply with the conditions of use of the model it is assumed that the flow through the holes are isentropic.

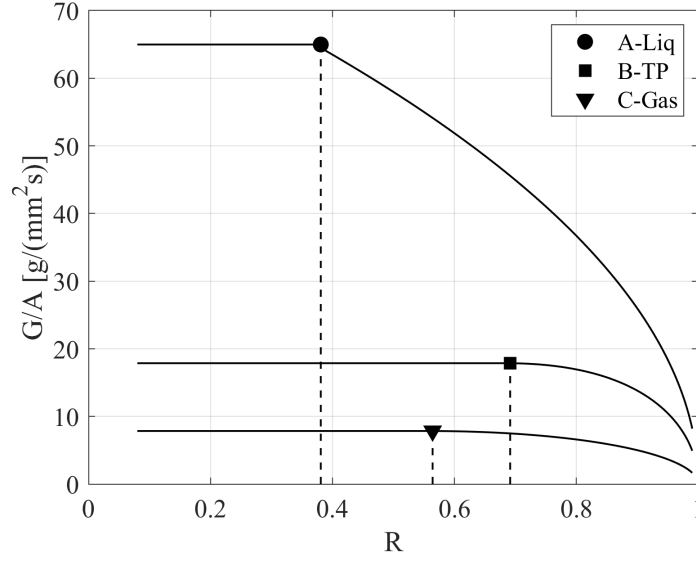


Figure 3.3. Development of the normalized mass flow rate for the 3 initial conditions in Figure 3.2 as a function of the expansion ratio.

Using the equations of conservation of mass, momentum and energy, the fluid velocity in the vena contracta (u_{vc}) is obtained:

$$u_{vc} = [(h^o - h_{is})]^{1/2} \quad (3.20)$$

Where h^o is the total upstream enthalpy and h_{is} is the enthalpy in the vena contracta.

Starting from the upstream total pressure (p^o), the fluid expand isentropically and the corresponding enthalpy (h_{is}), which depends on pressure variation and the upstream value of entropy, is evaluated. Figure 3.2 shows the trend of pressure and enthalpy during isentropic expansion, as described before, for 3 different initial conditions, liquid only (**A**), two-phase (**B**) and gas only (**C**). As the upstream pressure decreases, the mass flow rate increases until critical conditions are reached ($R_C = p_C/p^o$), where the flow rate reaches its critical value corresponding to:

$$\frac{G_{crit}}{A_{holes}} = \max(\rho \cdot u_{vc}) \quad (3.21)$$

with

$$A_{holes} = C_d \cdot \frac{\pi}{4} \cdot D_{holes}^2 \cdot N_{holes} \quad (3.22)$$

where C_d is the discharge coefficient of the hole, that has to be experimentally evaluated.

The trend of the mass flow rate for unit of area as a function of the expansion ratio ($R = p/p^o$), for the 3 cases previously mentioned are plotted in Figure 3.3. It can be noted how the criticality is reached with different expansion ratio depending on the starting condition. The critical conditions are also reported as the middle point for the processes in Figure 3.2. Consequently for a given upstream condition, if the expansion ratio is lower than critical ratio found, the nozzle is in critical conditions and the flow rate corresponds to this maximum, otherwise, no choking condition occurs and the flow rate is obtained through the subcritical isentropic efflux formulation.

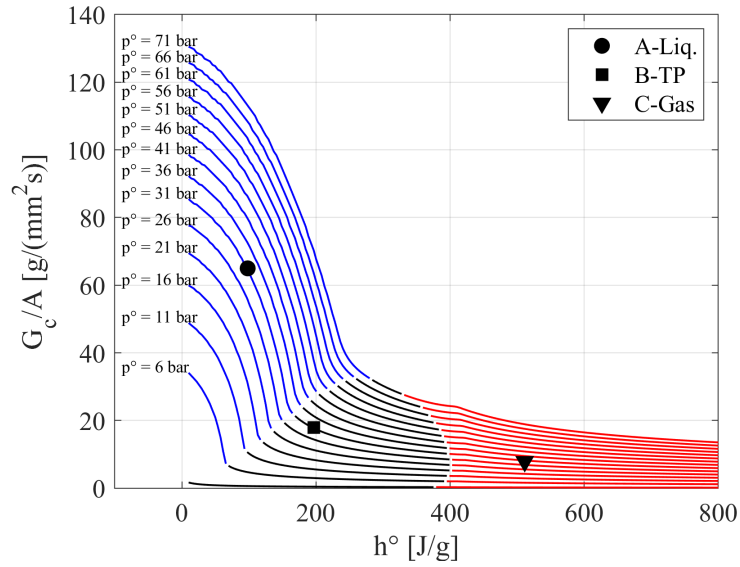


Figure 3.4. Specific mass flow trends as a function of upstream conditions (p^o h^o), in detail the points corresponding to the transformations in Figure 3.2.

Figure 3.4 shows the trends of the critical mass flow rate for unit of area as a function of the initial conditions. Each curve refers to a different total upstream pressure, and it should be noted that the flow rate decreases by increasing the total enthalpy. Note the three macro zones, in blue the subcooled liquid, in black the two-phase zone and in red the gas only.

3.4 Balloon energy conservation

Considering the control volume enclosed by the balloon (Figure 3.5) the equation is:

$$h_B - P_w/G = h_{out} + \frac{1}{2}u_{out}^2 \quad (3.23)$$

where, assuming the efflux kinetic energy is fully dissipated, h_B is the internal enthalpy of the balloon, P_w is the power absorbed by the system, G is the flow rate, h_{out} and u_{out} are the enthalpy and velocity at the exit in the balloon respectively.

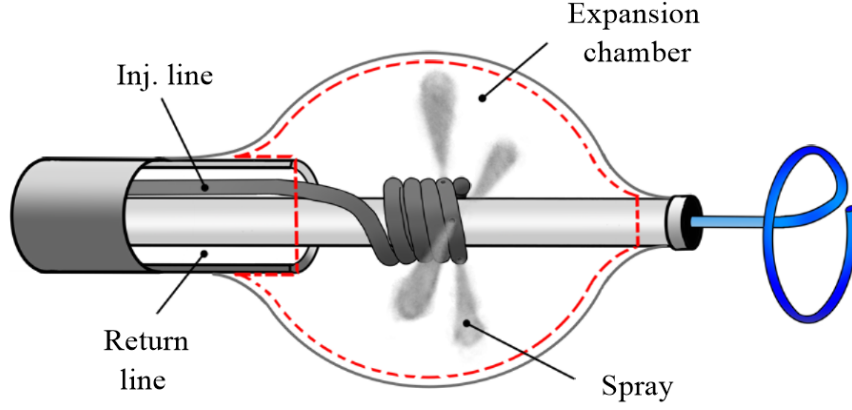


Figure 3.5. Schematic view of the balloon.

Consequently, as it can be deduced from the equation 3.23, in order to know the inlet conditions of the return line, P_w has to be defined. In the present thesis the stationary power exchanged is modeled as:

$$P_w = k_{ball} \cdot S_{ball} \cdot (T_{body} - T_{ball}) \quad (3.24)$$

S_{ball} is the total surface area of the balloon, T_{body} is the average human body temperature ($T_{body}=38^{\circ}\text{C}$), T_{ball} the internal temperature of the balloon during the ablation phase ($-40/-50^{\circ}\text{C}$ [43]).

Chapter 4

Phenomenological correlations

This section define the terms previously introduced, comparing the various models available to represent them and justifying the choice of one over another.

4.1 Friction models

As mentioned in equation 3.15, $\overline{\Delta p_{fw}}$ represents the Darcy-Weisbach equation. An empirical relation that links the pressure drop due to frictional force along a given length of pipe to the velocity and the average density of a fluid, where λ represents the Darcy coefficient, simply called friction factor. The evaluation of the friction

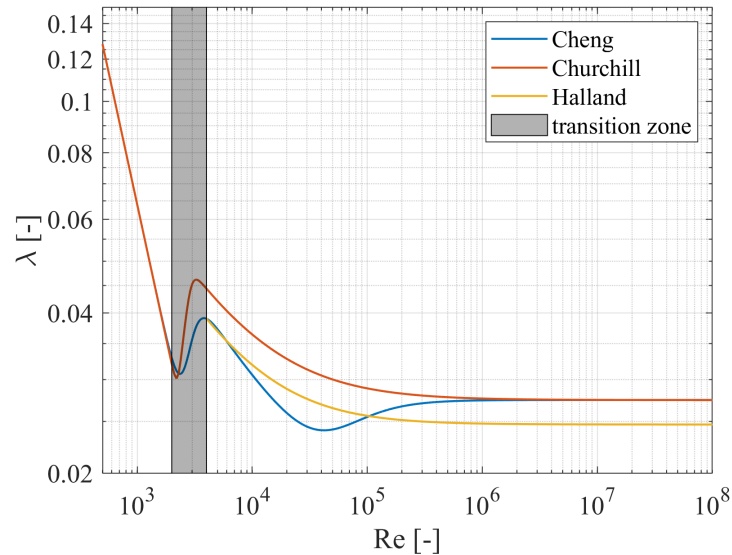


Figure 4.1. Trend of friction coefficient as a function of Reynolds number for $\epsilon/D = 3.5 \cdot 10^{-3}$ with different correlations.

coefficient depends on the fluid conditions, summarised by the Reynolds number:

$$Re = \frac{\rho \cdot d_h \cdot u}{\mu} \quad (4.1)$$

where d_h is the hydraulic diameter and μ the dynamic viscosity.

Due to homogeneity, there are no differences between the friction models for biphasic and mono-phasic fluid.

For numerical purposes, it is better to have a single function valid over the whole range of interest and without discontinuities, so only equations providing values for all regions, were considered. In the following a list of the most common ones:

Churchill(1977)[13]:

$$\lambda = 8 \left[\left(\frac{8}{Re} \right)^{12} + \frac{1}{(a+b)^{\frac{3}{2}}} \right]^{\frac{1}{12}} \quad (4.2)$$

$$a = \left\{ 2.457 \cdot \ln \left[\frac{1}{\left(\frac{7}{Re} \right)^{0.9} + 0.27 \left(\frac{\epsilon}{D} \right)} \right] \right\}^{16}$$

$$b = \left(\frac{37530}{Re} \right)^{16}$$

Haaland(1983)[24]:

$$\lambda = \left\{ -1.8 \cdot \log \left[\left(\frac{\epsilon/D}{3.7} \right)^{1.11} + \frac{6.9}{Re} \right] \right\}^{-2} \quad (4.3)$$

Cheng(2008)[10]:

$$\frac{1}{\lambda} = \left(\frac{Re}{64} \right)^a \left(1.8 \cdot \log \frac{Re}{6.8} \right)^{2(1-a)b} \left(2.0 \cdot \log \frac{3.7D}{\epsilon} \right)^{2(1-a)(1-b)} \quad (4.4)$$

$$a = \frac{1}{1 + \left(\frac{Re}{2720} \right)^9}$$

$$b = \frac{1}{1 + \left(\frac{Re \cdot \epsilon / D}{160} \right)^2}$$

In Figure 4.1, the trends of the different models are shown. It should be pointed out that in the range of $Re \leq 2300$, the laminar region, the various equations have the same trend. This is because in this region the coefficient of friction is equal to $64/Re$, with no dependence on diameter and roughness.

The range $2300 < Re < 4000$, highlighted in the figure, represents the transition zone, where the fluid assumes unstable behaviour and the friction coefficient is subject to a high uncertainty.

For $Re \geq 4000$ the fluid is in the turbulent region. In this case can be notes differences in the trends due to the different experimental sets used to derive the correlations.

In order to correctly assess which model to use, it is first necessary to analyse the dynamic viscosity models.

4.2 Dynamic viscosity models

Dynamic viscosity values, in mono-phasic region, are obtained as a function of pressure and enthalpy using *Refprop8*.

Using the homogeneous model simplifies the computational burden of the simulation, but appropriate correlations are required to calculate the liquid-vapour viscosity values from the saturation ones.

As already seen in equation 4.1, Re is inversely proportional to the dynamic viscos-

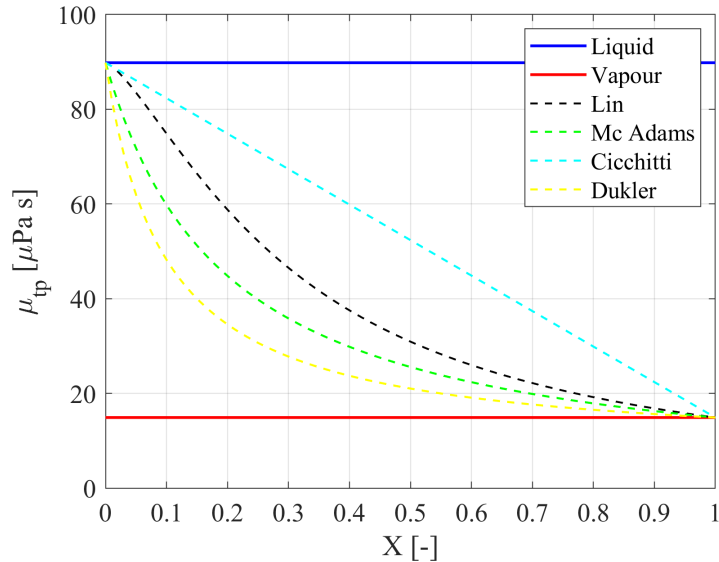


Figure 4.2. Trend of dynamic viscosity models for N2O at p=30 bar.

ity (μ), so in order to correctly predict the pressure drop during the phase transition, one must recognise the importance of using a viscosity model that best fits the case under consideration.

The most common found in literature are:

McAdams(1942)[33]:

$$\frac{1}{\mu_{tp}} = \frac{X}{\mu_v} + \frac{1-X}{\mu_l} \quad (4.5)$$

Cicchitti et al.(1959)[14]:

$$\mu_{tp} = (1-X) \cdot \mu_l + X \cdot \mu_v \quad (4.6)$$

Dukler, Wiks and Cleveland(1964)[19]:

$$\mu_{tp} = \frac{(1-X) \cdot \mu_l / \rho_l + X \cdot \mu_v / \rho_v}{(1-X) / \rho_l + X / \rho_v} \quad (4.7)$$

Lin et al.(1991)[31]:

$$\mu_{tp} = \frac{\mu_l \cdot \mu_v}{\mu_v + X^{1.4} \cdot (\mu_l - \mu_v)} \quad (4.8)$$

Where X is the quality, μ_l and μ_v are the dynamic viscosity for liquid and vapour respectively, while ρ_l and ρ_v are density for liquid and vapour respectively.

The quality (X) is defined as:

$$X = \frac{m_v}{m} \quad (4.9)$$

Where m is the total mass and m_v is the mass of vapour, so X will be 0 for a liquid and 1 for a gas. Given the dependence of the pressure trend by both the friction and the dynamic viscosity model, in order to decide the best combination, it will be necessary to compare the various correlation with experimental data.

4.3 Heat transfer correlations

The convective heat factor (\hat{h}) is directly proportional to the Nusselt number (Nu), which must be calculated for both lines in each volume into which the two domains have been divided. Since it depend on many factors, different relations are required to be defined from case to case, so both single and two-phase correlations are needed.

4.3.1 Single-phase

Knowing the system, as far as the single-phase case is concerned, different relations will be needed depending on the Reynolds number and the geometry, remembering that there are two coaxial tubes, so the flow will pass through a capillary and an annulus, while the outer surface of the return line is considered adiabatic. The models used, from [32] and [23], are :

For the capillary (simple pipe):

Laminar region ($Re < 2300$):

$$Nu_{s,L,1} = 3.66 \quad (4.10)$$

$$Nu_{s,L,2} = 1.615 \left(RePr \frac{d_i}{l} \right)^{1/3} \quad (4.11)$$

$$Nu_{s,L} = [Nu_{s,L,1}^3 + 0.7^3 + (Nu_{s,L,2} - 0.7^3)]^{1/3} \quad (4.12)$$

Turbulent case ($Re > 10^4$):

$$Nu_{s,T} = \frac{(\zeta_s/8)RePr}{1 + 12.7\sqrt{\zeta_s/8}(Pr^{2/3} - 1)} \left[1 + \left(\frac{d_i}{l} \right)^{2/3} \right] \quad (4.13)$$

$$\zeta_s = (1.8 \cdot \log_{10}(Re) - 1.5)^{-2} \quad (4.14)$$

Transitional region ($2300 < Re < 10^4$):

$$\gamma = \frac{Re - 2300}{10^4 - 2300} \quad (4.15)$$

$$Nu_s = (1 - \gamma)Nu_{s,L,2300} + \gamma Nu_{s,T,10^4} \quad (4.16)$$

For return line (annulus):

Laminar case ($Re < 2300$):

$$\zeta_{a,L} = 1.615[1 + 0.14(d_i/d_o)^{-1/2}] \quad (4.17)$$

$$Nu_{a,L,1} = 3.66 + 1.2(d_i/d_o)^{-0.8} \quad (4.18)$$

$$Nu_{a,L,2} = \zeta_{a,L}(RePrd_h/l)^{1/3} \quad (4.19)$$

Turbulent region ($Re > 10^4$):

$$Nu_{a,T} = \frac{(\zeta_{a,T}/8)RePr}{1 + 12.7\sqrt{\zeta_{a,T}/8}(Pr^{2/3} - 1)} \left[1 + \left(\frac{d_h}{l} \right)^{2/3} \right] F_a K \quad (4.20)$$

$$\zeta_{a,T} = (1.8 \cdot \log_{10} Re^* - 1.5)^{-2} \quad (4.21)$$

$$Re^* = Re \frac{(1 + a^2)\ln(a) + (1 - a^2)}{(1 - a)^2 \ln(a)} \quad (4.22)$$

$$a = \frac{d_i}{d_o} \quad (4.23)$$

$$F_a = 0.86a^{-0.16} \quad (4.24)$$

$$K = (Pr/Pr_w)^{0.11} \quad (4.25)$$

Transitional region ($2300 < Re < 10^4$):

$$Nu_a = (1 - \gamma)Nu_{a,L,2300} + \gamma Nu_{a,T,10^4} \quad (4.26)$$

where Pr and Pr_w are the Prandtl number at bulk and at wall temperature respectively.

4.3.2 Two-phase

Inside the capillary, due to a pressure drop or heat exchange, a second phase may be present, as well as in the return line if the balloon does not exchange enough heat with the body.

In order to simulate these specific cases as well, it was necessary to implement a model for the Nusselt number in the case of evaporation.

Phase transition - **Evaporation:**

Li and Wu(2010)[30]:

$$Nu_{tp} = 22.9(Bo \cdot Re_l^{0.5})^{0.355} \quad (4.27)$$

where Re_l is the liquid Reynolds number

$$Re_l = \frac{G(1-X)d_h}{\mu_l} \quad (4.28)$$

and Bo is the Bond number, defined as:

$$Bo = \frac{g(\rho_l - \rho_v)d_h^2}{\sigma} \quad (4.29)$$

The relationship was chosen because it was specifically validated for diameters in the range 0.2-3 mm and tested for 12 working fluids such as $R12$ and CO_2 , but not for N_2O , for which no data were found.

To complete the case study, the case where there is a phase transition from gas to liquid must be considered. In literature can be found different ways to describe this kind of event, the most common are:

Phase transition - **Condensation:**

Akers(1960)[1]:

$$Nu_{tp} = 0.026 \cdot Pr_l^{1/3} \left\{ G \left[(1-X) + X \left(\frac{\rho_l}{\rho_v} \right)^{0.5} \right] \frac{D_h}{\mu_l} \right\}^{0.8} \quad (4.30)$$

Cavallini and Zecchin(1974):[8]

$$Nu_{tp} = 0.05 \cdot Re_l^{0.8} \cdot Pr_l^{0.33} \left[1 + \left(\frac{\rho_l}{\rho_v} \right)^{0.5} \left(\frac{X}{1-X} \right) \right]^{0.8} \quad (4.31)$$

Bohdal, Charun, and Sikora(2011)[4]:

$$Nu_{tp} = 25.084 \cdot Re_l^{0.258} \cdot Pr_l^{-0.495} \cdot p_{red}^{-0.288} \cdot \left(\frac{X}{1-X} \right)^{0.266} \quad (4.32)$$

Shah(2016)[41]:

$$Nu_{tp} = 0.023 \cdot Re_l^{0.8} \cdot Pr_l^{0.4} \cdot \left(1 + \frac{3.8}{Z^{0.95}}\right) \left(\frac{\mu_l}{14\mu_v}\right)^{(0.0058+0.557p_{red})} \quad (4.33)$$

$$Z = (1/X - 1)^{0.8} \cdot p_{red}^{0.4} \quad (4.34)$$

where Pr_l is the only liquid Prandtl number and p_{red} is the reduced pressure defined as $p_{red} = p/p_c$ with p_c as the critical pressure. Despite the fact that this is a widely studied topic, in literature there are no models for the substance in use. Because of the high uncertainty of such correlations no correct one exist. The one presented by Shah was chosen because is the one commonly used and it has been tested for many cryogenic fluids, although not the one used by the probe.

Chapter 5

Solving method

As already stated the equations have been discretized following the finite volume method, it remains to be defined how the division of the domain has been carried out.

The formulation used to discretize the domain is:

$$\Delta x_i = \frac{L}{\tanh(k)} \left[\tanh\left(k \frac{i}{N}\right) - \tanh\left(k \frac{i-1}{N}\right) \right] \quad (5.1)$$

where N is the number of desired elements, Δx_i indicates the length of the i -th control volume which is a function of the parameter k and L is the total length to be discretized. The Fig.5 shows the trend of Δx as a function of k .

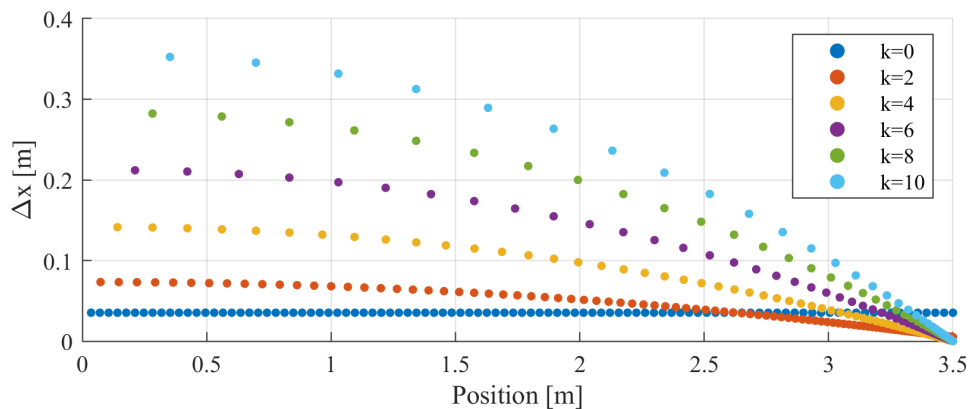


Figure 5.1. Trends of length Δx as a function of position, when parameter k varies for $L=3.5$ m e $N=100$.

The greater k the more points will be distributed in the final part of the length,

this is useful for a correct modelling because in the modelling of tubular expansion systems for cooling, near the outlet section is where the fluid reaches criticality, this event is characterised by a pressure gradient that tends to infinity.

This subdivision is used for the capillary, while for the return line the trend of Δx is the reverse.

Before going on to show the set of equations, it is necessary to introduce the minor pressure losses. They are due to obstacles such as bends, elbows or as in this case to the narrowing of the pipeline. The equation is:

$$\Delta p = \frac{1}{2}\beta\rho u^2 \quad (5.2)$$

where β is the minor losses factor. In cases of pipe narrowing, such as in the transition between the pre-cooler and the capillary or from the cryoballoon to the return line $\beta = 0.5$.

All the elements of the model have been defined, so it is possible to write the complete set of non-linear equations that will need to be solved.

Capillary

Inlet conditions $i=1$;

$$\mathbf{f}_{C,1} = \begin{pmatrix} p_{C,1} - p_0 + \frac{1}{2}\beta\rho_{C,1}u_{C,1}^2 \\ h_{C,1} + \frac{1}{2}u_{C,1}^2 - h_0 \\ \rho_{C,1} - f_s(p_{C,1}, h_{C,1}) \\ \rho_{C,1}u_{C,1} - \frac{G}{A_C} \end{pmatrix}^T = 0 \quad (5.3)$$

$2 \leq i \leq N$

$$\mathbf{f}_C = \begin{pmatrix} \rho_{C,i} \cdot u_{C,i}^2 - \rho_{C,i-1} \cdot u_{C,i-1}^2 + p_{C,i} - p_{C,i-1} + \overline{\Delta p_{fw,C,i}} \\ h_{C,i} + \frac{1}{2}u_{C,i}^2 - h_{C,i-1} - \frac{1}{2}u_{C,i-1}^2 + \frac{Q_{w,C,i}}{G} \\ \rho_{C,i} - f_s(p_{C,i}, h_{C,i}) \\ \rho_{C,i} \cdot u_{C,i} - \rho_{C,i-1} \cdot u_{C,i-1} \end{pmatrix}^T = 0 \quad (5.4)$$

Orifices

if $\frac{p_B}{p_N} \leq R_{crit}$

$$\mathbf{f}_g = (G - G_{crit}) = 0 \quad (5.5)$$

if $\frac{p_B}{p_N} > R_{crit}$

$$\mathbf{f}_g = (G - A_{holes} \cdot \rho_B \cdot u_{vc}) = 0 \quad (5.6)$$

Velocity in the vena contracta

$$\mathbf{f}_{vc} = \left(u_{vc} - \left(h_{C,N} + \frac{1}{2}u_{C,N}^2 - h_{vc} \right)^{\frac{1}{2}} \right) = 0 \quad (5.7)$$

Balloon equation

$$\mathbf{f}_B = \left(h_B - P_w/G - h_{R,1} - \frac{1}{2}u_{R,1}^2 \right) = 0 \quad (5.8)$$

Absorbed power

$$\mathbf{f}_{Pw} = \left(P_w - k_{ball} \cdot S_{ball} \cdot (T_{body} - T_{ball}) \right) = 0 \quad (5.9)$$

Return line

 Inlet conditions $i=1$

$$\mathbf{f}_{R,1} = \begin{pmatrix} p_{R,1} - p_B + \frac{1}{2}\beta\rho_{R,1}u_{RL,1}^2 \\ h_{R,1} + \frac{1}{2}u_{R,1}^2 - h_B \\ \rho_{R,1} - f_s(p_{R,1}, h_{R,1}) \\ \rho_{R,1}u_{R,1} - \frac{G}{A_R} \end{pmatrix}^T = 0 \quad (5.10)$$

 $2 \leq i \leq N$

$$\mathbf{f}_R = \begin{pmatrix} \rho_{R,i} \cdot u_{R,i}^2 - \rho_{R,i-1} \cdot u_{R,i-1}^2 + p_{R,i} - p_{R,i-1} + \overline{\Delta p_{fw,R,i}} \\ h_{R,i} + \frac{1}{2}u_{R,i}^2 - h_{R,i-1} - \frac{1}{2}u_{R,i-1}^2 - \frac{Q_{w,R,i}}{G} \\ \rho_{R,i} - f_s(p_{R,i}, h_{R,i}) \\ \rho_{R,i} \cdot u_{R,i} - \rho_{R,i-1} \cdot u_{R,i-1} \end{pmatrix}^T = 0 \quad (5.11)$$

Pressure valve

$$\mathbf{f}_p = \left(p_{R,N} - p_{valv} \right) = 0 \quad (5.12)$$

So:

$$\mathbf{f}(\mathbf{x}) = \left(\mathbf{f}_C \ \mathbf{f}_g \ \mathbf{f}_{vc} \ \mathbf{f}_B \ \mathbf{f}_{Pw} \ \mathbf{f}_R \ \mathbf{f}_p \right)^T = 0 \quad (5.13)$$

 Where \mathbf{f} is the vector of functions and \mathbf{x} is the vector of unknown variables defined by:

$$\mathbf{x}_C = \left(p_{C,1} \ h_{C,1} \ \rho_{C,1} \ u_{C,1} \ \dots \ p_{C,i} \ h_{C,i} \ \rho_{C,i} \ u_{C,i} \ \dots \ p_{C,N} \ h_{C,N} \ \rho_{C,N} \ u_{C,N} \right)^T ; \quad (5.14)$$

$$\mathbf{x}_R = \left(p_{R,1} \ h_{R,1} \ \rho_{R,1} \ u_{R,1} \ \dots \ p_{R,i} \ h_{R,i} \ \rho_{R,i} \ u_{R,i} \ \dots \ p_{R,N} \ h_{R,N} \ \rho_{R,N} \ u_{R,N} \right)^T \quad (5.15)$$

$$\mathbf{x}_B = \left(G \ p_B \ h_B \ u_{vc} \ P_w \right)^T \quad (5.16)$$

The vector of variables is represented by :

$$\mathbf{x} = \left(\mathbf{x}_C \ \mathbf{x}_B \ \mathbf{x}_R \right)^T \quad (5.17)$$

Finally the number of non-linear equations to be solved (\tilde{N}) corresponds to:

$$\tilde{N} = 2 \cdot 4 \cdot N + 5 \quad (5.18)$$

where 4 is the number of basic equations multiplied by 2, the number of lines, N the number of elements into which the system was divided and 5 the number of accessory equations: mass flow rate, velocity in the vena contracta, balloon energy equation, balloon thermal power exchanged and final pressure of the return line.

The above set of equations have been solved by the Newton-Rapshon method. The resolution consists of an iterative procedure where $\mathbf{x}^{(j)}$ is the vector of approximate solutions at the j -th iteration.

Consequently the method can be summarised as:

$$\mathbf{J}^{(j)} \Delta \mathbf{x}^{(j)} = -\mathbf{f}(\mathbf{x}^{(j)}), j = 0,1,2, \dots \quad (5.19)$$

so:

$$\mathbf{x}^{(j+1)} = \mathbf{x}^{(j)} + \Delta \mathbf{x}^{(j)}, j = 0,1,2, \dots \quad (5.20)$$

where $\Delta \mathbf{x}$ is the vector of corrections and $\mathbf{J}^{(j)}$ is the Jacobian matrix defined as:

$$\mathbf{J}^{(j)} = \mathbf{J}(\mathbf{x}^{(j)}) = \begin{pmatrix} \left(\frac{\partial f_1}{\partial x_1} \right) & \left(\frac{\partial f_1}{\partial x_2} \right) & \dots & \left(\frac{\partial f_1}{\partial x_{\tilde{N}}} \right) \\ \left(\frac{\partial f_2}{\partial x_1} \right) & \left(\frac{\partial f_2}{\partial x_2} \right) & \dots & \left(\frac{\partial f_2}{\partial x_{\tilde{N}}} \right) \\ \vdots & \vdots & \ddots & \vdots \\ \left(\frac{\partial f_{\tilde{N}}}{\partial x_1} \right) & \left(\frac{\partial f_{\tilde{N}}}{\partial x_2} \right) & \dots & \left(\frac{\partial f_{\tilde{N}}}{\partial x_{\tilde{N}}} \right) \end{pmatrix} \quad (5.21)$$

The two equations (5.19) and (5.20) define Newton's method, starting from an initial approximate solution vector $\mathbf{x}^{(0)}$ and by imposing the fluid inlet condition p_0 and h_0 , the temperature of the human body (T_{body}) and the pressure at the end of the return line (p_{valv}), the iterative process determines a succession of approximations $\{\mathbf{x}^{(j)}\}$ converging to solution of the model.

Chapter 6

Comparison of friction and dynamic viscosity models

In chapter 4 different friction and viscosity models have been defined. In the following section combination of the listed models have been analysed to find the most suitable pair. The experimental work [40] was chosen as a reference.

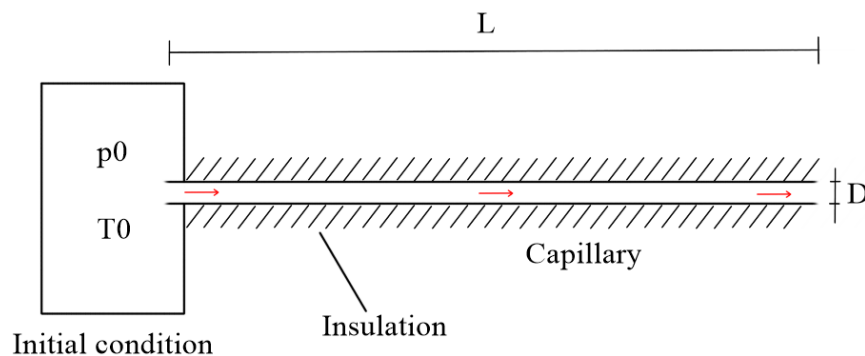


Figure 6.1. Schematic representation of the capillary.

The interest in capillary tubes is due to their wide use in refrigeration systems, in the papers in which it is treated, the focus is on the evaluation of the maximum flow rate that can be disposed of by a given capillary at given starting states, thus focusing mainly on the study of the critical conditions reached by the fluid and the point where the phase change due to expansion begins.

For this purpose, as shown in the Figure 6.1 an adiabatic capillary was modelled, using the same method as for the probe, excluding the heat transfer, the holes and

the balloon equation.

For this specific case, the critical flow rate of the capillary was derived by iteration, checking the conditions of choking in the last control volume, which according to [3] are reached when the entropy of the refrigerant tends to decrease ($\Delta s < 0$), or as stated in [20], when the pressure gradient approaches to infinity ($dp/dx \rightarrow \infty$). If these conditions occur in a previous volume, it is needed to reduce the mass flow rate, while if criticality is not reached, flow has to be increase.

The evaluation was carried out by implementing the various combinations of the friction and viscosity models, reproducing the experiments shown in [40], corresponding to the conditions summarised in the table 6.1. The results obtained were then compared with the measured values.

The the critical mass flow rate values obtained were compared with the measured value analysing the Relative Error (RE):

$$RE = \frac{G_{C,exp} - G_{C,sim}}{G_{C,sim}} \quad (6.1)$$

while the pressure gradient was compared with the experimental values using the Root Mean Square Deviation (RMSD):

$$RMSD = \sqrt{\sum \frac{(p_{i,Sim} - p_{i,Exp})^2}{N_p}} \quad (6.2)$$

Comparison of the results showed, that the error in the critical flow rate disposed of varied from a maximum of 10% to a minimum of 1%. Whereas with regard to pressure trends, the deviation ranged from a maximum of 0.9 bar to a minimum of 0.1 bar.

	L	D	p_i	T_i
A	1.5 m	0.66 mm	9.67 bar	31.4°C
B	1.5 m	0.66 mm	7.17 bar	23.4°C
C	1.5 m	1.17 mm	8.85 bar	30.0°C
D	1.5 m	1.17 mm	8.40 bar	33.8°C
E	1.83 m	1.41 mm	8.56 bar	32.5°C

Table 6.1. Input data for the simulation [40].

Considering the measurement error band, which is not provided by the author, and

the narrow range of errors, it is not possible to state with certainty the best combination to use, for this reason the choice was purely subjective, selecting Cheng as the friction model and Lin for the dynamic viscosity.

The results for the chosen pair of models will now be shown.

	$\frac{G_{C,exp}}{A} [\frac{kg}{sm^2}]$	$\frac{G_{C,sim}}{A} [\frac{kg}{sm^2}]$	RE [%]	$RMSD$ [bar]
A	3306	3099	6.3	0.21
B	2468	2321	4.4	0.13
C	4046	3932	3.5	0.80
D	3164	3084	2.4	0.26
E	3778	3471	8.8	0.26

Table 6.2. Results comparison between experimental and simulated values.

As can be seen from the the table 6.2, the simulation gives a good approximation of the value of critical mass flow rate with an error lower than 10%.

Regarding the pressure trend, looking at the results in Figure 6.3 for **A-B-D** and in Figure 6.3 for case **E**, the simulation gives a good approximation of the pressure drop, the critical case seems to be trend **C**.

In case **C** can be seen that the pressure drop is slightly underestimated, assuming that the geometric data provided are nominal values, this error could be due to a different absolute roughness, as no information is provided or an error due to the unknown band of error.

The change in the pressure trend is due to the continuous expansion inside the capillary, which brings the fluid to a saturated condition. As the fluid evaporates, it reduces its density and accelerates, increasing the pressure reduction.

This section demonstrates the model's ability to evaluate pressure drops within a capillary, hence it can be used for cryoprobe modelling.

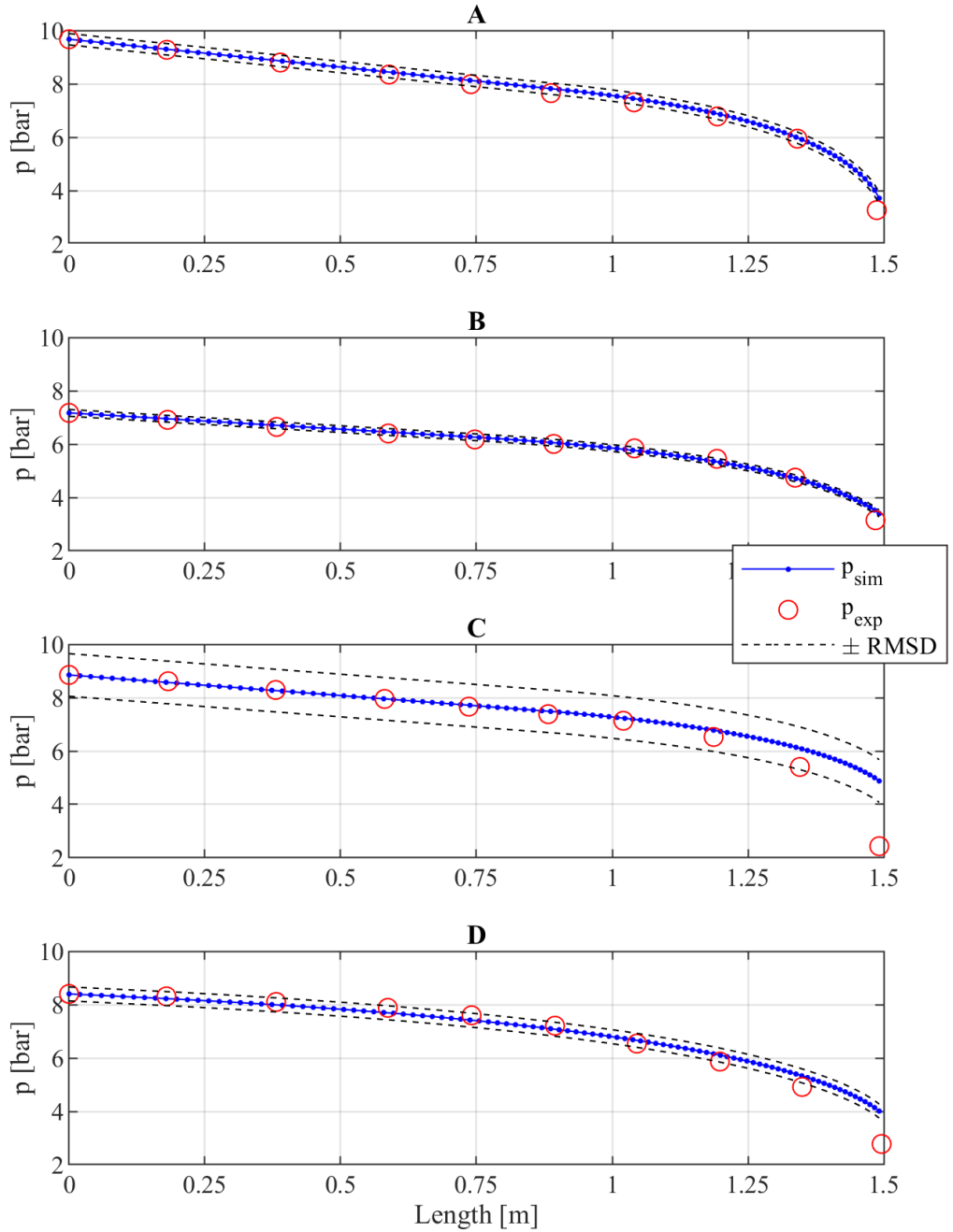


Figure 6.2. Comparison of experimental simulated pressure trends for the conditions described in table 6.1 from A to D

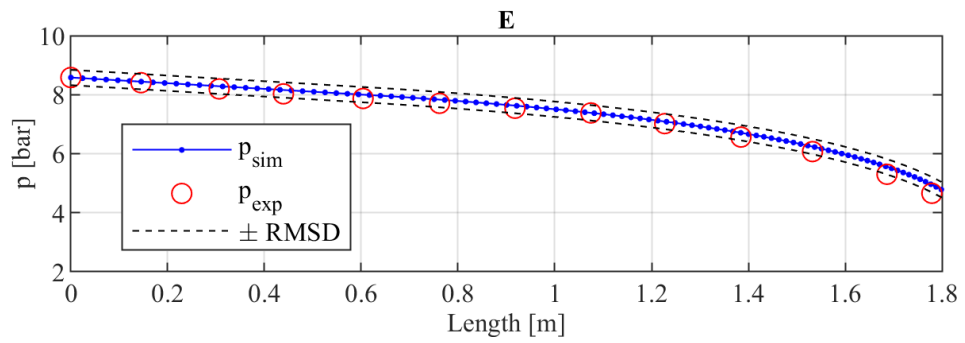


Figure 6.3. Comparison of experimental simulated pressure trends for the condition described in table 6.1 case E

Chapter 7

Experimental Setup

To validate the proposed model, an experimental campaign has been realized. The experimental bench was set in order to work with fluid under three different states: gas-only, sub-cooled liquid and two-phase.

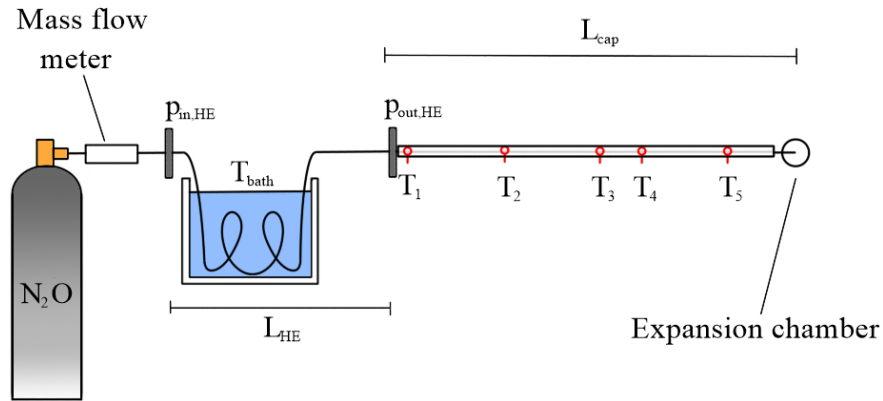


Figure 7.1. Schematic representation of the experimental setup.

A schematic diagram of the test bench is shown in the Figure 7.1. Starting from a pressurized reservoir containing N_2O , a steel tube leads to a thermal mass flow meter (Bronkhorst FG-211CV), followed by a heat exchanger consisting of a section of tube of length L_{he} immersed in a isothermal bath of glycole. The temperature of the bath can be adjusted in order to set the desired inlet condition of measurement. Two pressure transducers (Trafag NAT8252) are placed upstream and downstream of the exchanger in order to assess the pressure drop of the section. The heat exchanger is connected to the capillary representing the probe without the return line. The capillary is made of stainless-steel ($k_{steel}=17$ W/ mK) and a length of $L_{cap}=1.8$ m with an internal diameter of 1.1 mm and a thickness of 0.2 mm. A 10

cm layer of polyurethane foam ($k_{ins}=0.034$ W/mK), insulate it.

Five thermocouples were positioned along the length of the capillary, the first, together with the pressure sensor upstream of the probe, provides the input information for the simulation, while the others provide the temperature trend inside the capillary.

At the end of the capillary, 4 holes of $d_{holes}=65$ μm were made using laser drilling. The holes allow the fluid to expand inside a transparent expansion chamber connected to the vent line.

Heat exchanger preliminary dimensioning

In order to design the heat exchanger, the model of the probe has been modified. It was considered only the capillary part equations 5.3 and 5.4, creating a model that works using mass flow rate, initial temperature and pressure as input parameters and provides the heat exchanger length as output.

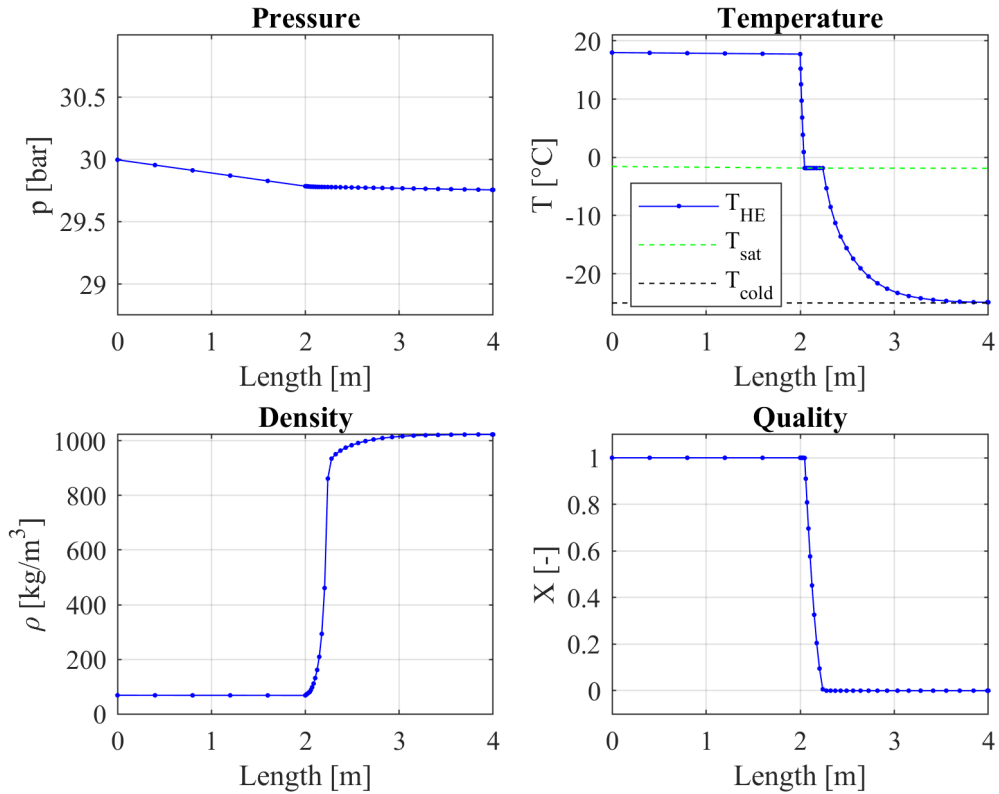


Figure 7.2. Simulation results: $p_0=30$ bar, $T_0=18$ °C $G=204$ mg/s
 $T_{cold}=-25$ C° $L_{HE}=4$ m.

As input conditions, were used ambient temperature ($T_0=18^\circ\text{C}$) and a pressure of $p_0=30$ bar. While for the tube, a stainless-steel one with an internal diameter of 1.05 mm and a thickness of 0.2 mm has been used.

Once the input conditions have been defined, the values to be achieved must be determined. In a Medtronic patent [47] about cryoballoon, data on the range of flow rate (around 200 mg/s) and inlet temperature ($-25/-30^\circ\text{C}$) of the probe under ablation conditions have been derived.

As can be seen from the schematic of the experimental bench (Figure 7.1), it is not possible to connect the thermal bath directly to the reservoir, so it is necessary to simulate an additional 2 m of tube that will exchange with the environment. Considering a pre-cooler temperature of $T_{cold}=-25^\circ\text{C}$, the simulation result is shown in Figure 7.2. Observing the temperature trend, it can be seen that at least 4 m are needed to bring the temperature down to T_{cold} . As can be seen from the quality, 20 cm are required for the condensation of the fluid.

As before, for reasons of connections, it is necessary to consider an additional metre connecting the thermal bath to the capillary. Considering the worst case, it is assumed that it exchanges directly with the environment.

Therefore, to obtain the desired conditions it is necessary to reduce the temperature of the thermal bath to $T_{cold}=-50^\circ\text{C}$.

Consequently, a new simulation was carried out to evaluate the length of the heat exchanger.

Considering as the length of the heat exchanger the sum of the immersed and air sections, as can be seen from the temperature plot of the simulation (Figure 7.3), the required length is 6 m and the final air exchange section has an high influence on the conditions of the fluid entering the capillary, in the case under consideration this affects the temperature of the fluid to rise by 25°C .

Looking at the pressure trend, it can be seen that the phase change affects the pressure trend. An increase in density leads to a reduction in velocity, which reduces the pressure drop.

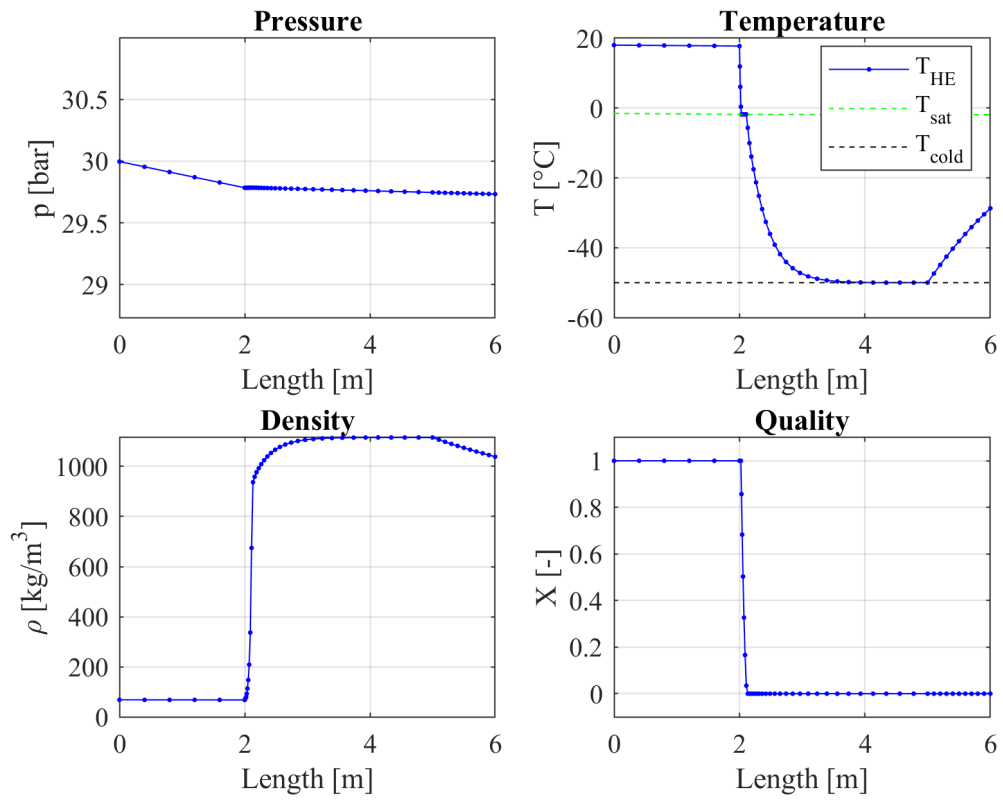


Figure 7.3. Simulation results with the last meter that exchanges in the air : $p_0=30$ bar, $T_0=18$ °C $G=204$ mg/s $T_{cold}=-50$ C° $L_{HE}=6$ m

Chapter 8

Results and Discussion

In order to carry out the various measurements, the inlet pressure of the capillary was varied between 10 and 32 bar, while the temperature was varied between 18.5°C and -43°C, in order to obtain different fluid conditions inside the capillary.

Setting the temperature of the thermal bath, the different measurements for each point were taken by waiting for the fluid to reach and maintain stationarity, and then averaging in the last 100 s of the measurement.

The derived data will then be compared with the numerical values obtained from the model.

To adapt the simulations to the experimental setup, the return line was neglected, a 10 cm layer of insulation (s_{ins}) was placed around the capillary and a model for natural convection (\hat{h}_{air}) in air at room temperature was implemented to evaluate the temperature trend inside the capillary under the setup conditions. The transmittance becomes:

$$U = \left[\frac{1}{\hat{h}_{IL}} + \frac{s_{IL} \cdot \ln(A_o/A_i)}{k_{steel} \cdot (A_o - A_i)} + \frac{s_{ins} \cdot \ln(A_{ins}/A_i)}{k_{iso} \cdot (A_{ins} - A_i)} + \frac{A_i}{\hat{h}_{air} \cdot A_{ins}} \right]^{-1} \quad (8.1)$$

The heat transfer of the balloon was neglected ($k_{ball}=0$) and the capillary was divided into N=100 elements with a k=2.5.

This experimental bench does not allow the model to be fully validate, but it allows validation of the flow model and the heat transfer model modified to simulate experimental conditions.

Figure 8.1 shows the comparison between the simulated mass flow values (G_{sim}) and the experimental ones (G_{exp}). As can be seen, the results obtained fall within the error range of $\pm 10\%$.

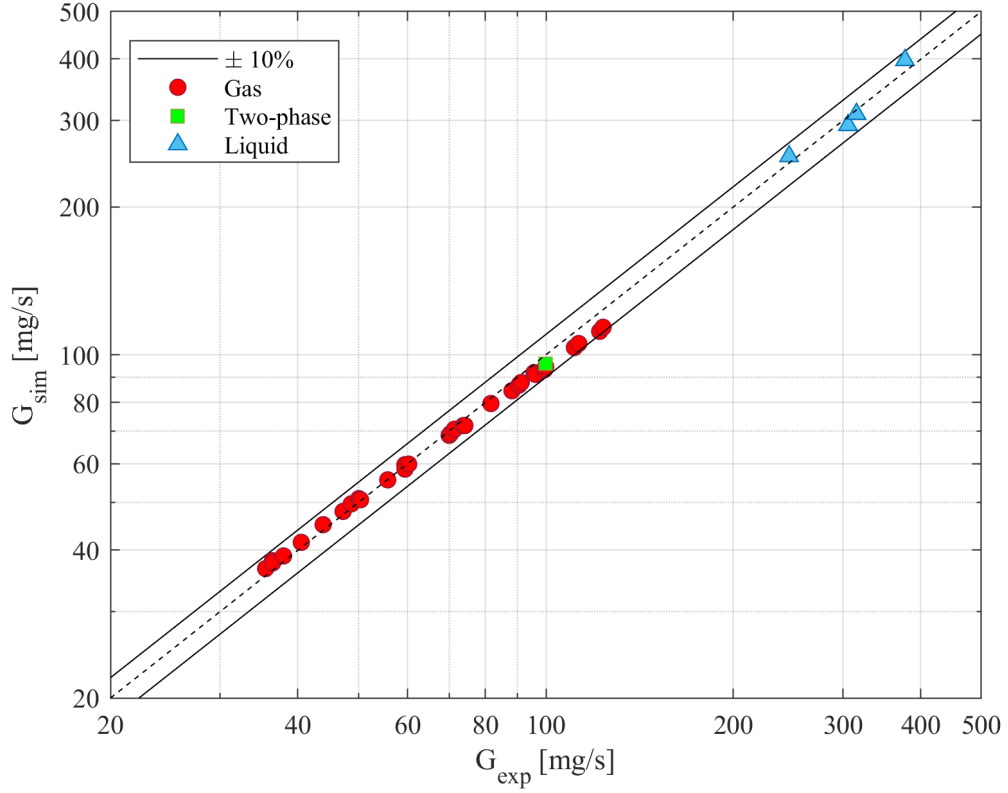


Figure 8.1. Comparison of measured vs simulated mass flow rate

Three cases will now be shown as examples, one for each fluid working condition: gas only, two-phase and subcooled liquid. The quality of the fluid was assessed by analysing the numerical results of simulations and temperature measurements along the capillary.

Gas-only

With regard to the measurements under gas-only conditions, the thermal bath was set at ambient temperature ($T_{cold}=18.5$ °C).

In Figure 8.2, a) shows the experimental trend of pressures, temperatures and mass flow rate.

In the various trends, a transient and a stationary trait can be distinguished. The first one is not taken into account as it represents an unstable fluid, to determine the actual experimental values it is averaged over the second one where the fluid is stable, yielding the values, $p_{out,HE}=23.7$ bar, $T_1=18.5$ °C and $G_{exp}=81.9$ mg/s.

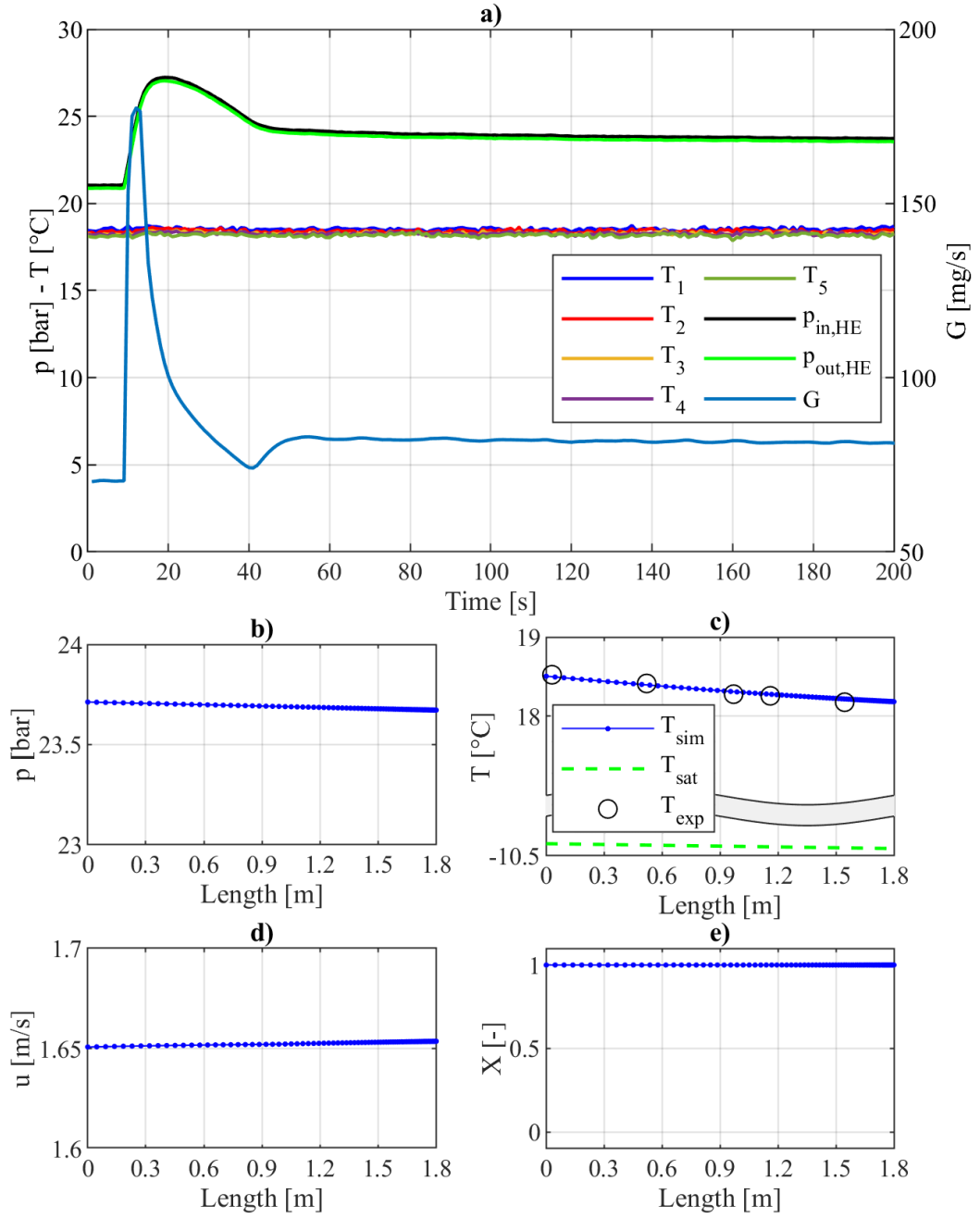


Figure 8.2. **a)**: Experimental $T_{cold}=18$ °C. **[b-c-d-e)**: Capillary simulation with input value, experimentale temperatures and mass flow rate obtained from **a)** averaging in the last 100s ($p_0=23.7$ bar, $T_0=18.5$ °C and $G=81.9$ mg/s).

The simulation was carried out using the conditions measured upstream of the capillary in order to compare the flow rate values and the temperature trend.

Looking at **b)**, where the calculated pressure trend is shown, there are no gradient variations typical of a phase change. In **c)** is plotted the calculated temperature trend (T_{sim}) with the relative saturation condition (T_{sat}) and the temperature values (T_{exp}) obtained from the measurements **a)**. The simulated temperature, in accordance with the experimental ones, does not meet the saturation value, it can be observed only a slightly reduction of temperature due to the fluid expansion. As seen in **b)** and **c)** it is possible to state that the fluid is in a gas-only condition. The graph **d)** where the quality is shown, confirms the statement showing a constant trend equal to $X = 1$ that corresponds to the quality value for only-gas. In **d)** is shown an increasing in the velocity, in accordance with the pressure drop trend. The flow rate value obtained corresponds to $G_{sim}=80$ mg/s, with an error of 2.4% with respect to the measured value.

Two-phase

For the two-phase fluid conditions, a single measurement session was made, imposing the temperature of the thermal bath at -30°C .

The graph **a)** in Figure 8.3, as in the previous case, shows the trend of p , T and G . Observing the pressure values, it can be seen that after an initial unstable trend, it shows a slightly decreasing trend, which has been neglected.

Looking at the temperature trends, it can be seen that $T_3-T_4-T_5$ have the same temperature, this is due to reaching the evaporation temperature. This event implies the nucleation of bubbles, which could affect the flow of the fluid and the passage through the holes. In fact, observing the plot of the flow rate measurements (G), a slightly oscillatory trend can be seen.

For this case, the experimental values obtained from the plot are: $p_{out,HE}=25.1$ bar, $T_1=-15^{\circ}\text{C}$ and $G_{exp}=100.0$ mg/s.

The simulation results are shown in the the graphs **b-c-d-e** of Figure 8.3. Starting from **c)**, the calculated temperature trend is in accordance with the experimental values. The simulated temperature reaches saturation conditions at around 1.0 m, confirming that the evaporation temperature has been reached. The phase change is confirmed by the quality trend shown in **e)**, which shows a change from liquid-only conditions $X=0$, reaching a value of around $X=0.1$ at the end of the capillary. Looking graph **d)**, it can be seen that the fluid accelerates as soon as evaporation conditions are reached. A slight change in quality is enough to influence the velocity. While from Figure **b)** can be noted that pressure does not seem to be affected

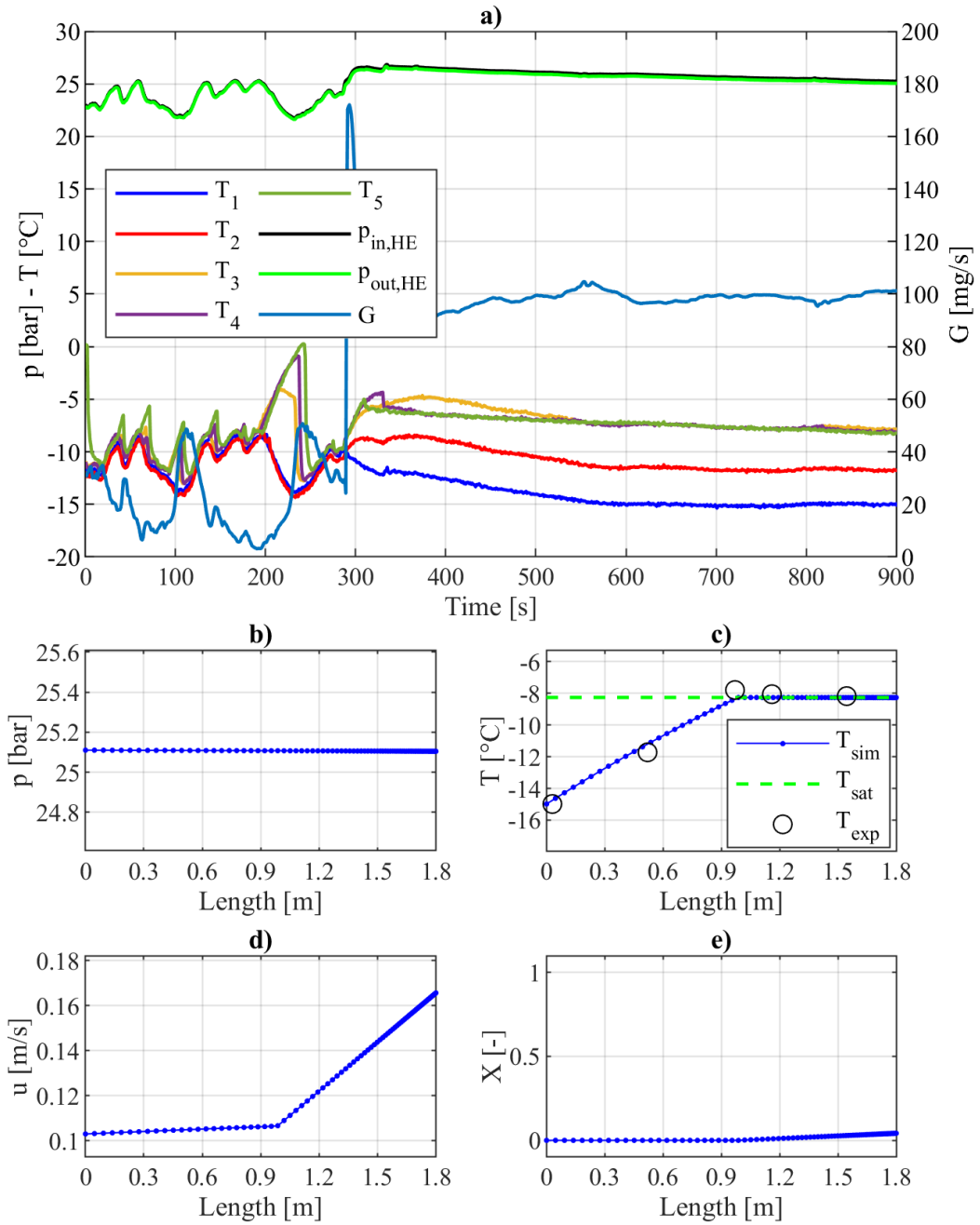


Figure 8.3. **a)**: Experimental $T_{cold}=-30$ °C. **[b-c-d-e)**: Capillary simulation with input value, experimental temperatures and mass flow rate obtained from **a)** averaging in the last 100s ($p_0=25.1$ bar, $T_0=-15$ °C and $G=100$ mg/s).

by the appearance of the second phase, probably due to the low percentage of gas. In this case a flow rate of $G_{sim}=96$ mg/s was obtained, which deviates by -4.1% from the measured value.

Liquid-only

To obtain a series of measurements under liquid-only conditions, the bath was setted at a temperature of $T_{cold}=-60$ °C.

The graph **a)** in Figure 8.4, shows one of the measurement sessions carried out in subcooled liquid condition, with the various trends obtained from the sensors. It should be noted that in liquid only condition, the thermocouple measurements attain stationarity along 5 distinct temperature values depending on their positions. This shows the increasing temperature trend along the capillary.

In this case the averaged values are: $p_{out,HE}=25.3$ bar, $T_1=-39.7$ °C and $G_{exp}=377$ mg/s.

Using the data obtained as input, graphs **b-c-d-e** in Figure 8.4 were obtained. Starting from graph **c)**, the simulated temperature trend and the experimental values are in accordance. Is evident from simulated and experimental values that the temperature of the fluid does not reach saturation conditions. This is confirmed by graph **e)** representing quality, where the trend is constant and equal to $X=0$. The plotted velocity in graph **d)** shows no change in its trend, which means that the density does not vary significantly, confirming the absence of phase change. Looking at graph **b)** representing the pressure, one can only notice a slight drop in pressure, due to the passage of the fluid. Its constant trend indicates that there is no noteworthy change in the state of the fluid. In fact, as already stated, for the simulation, the fluid remains in the condition of a subcooled liquid. In this case a flow rate of $G_{sim}=399$ mg/s was calculated, which deviates by 5.5% from the measured value.

As already stated by showing graph 8.1, even when looking at individual cases, the mass flow values are within a range of $\pm 10\%$ of the measured ones, which allows the flow model to be validated. The calculated temperature trends under the various conditions are in accordance with the measured values, thus validating the modified heat transfer model for the experimental set up.

Looking in particular at the temperature trends of the two-phase case and the liquid-only case (graph **c)** in Figure 8.3 and 8.4. It can be seen that despite the expansion, they have an increasing trend. The increase evaluated for both cases is about 7°C, which demonstrates an evident exchange with the outside, consequently the insulation is an element to be improved on the bench.

These measurements do not allow the model to be fully validated. A different test

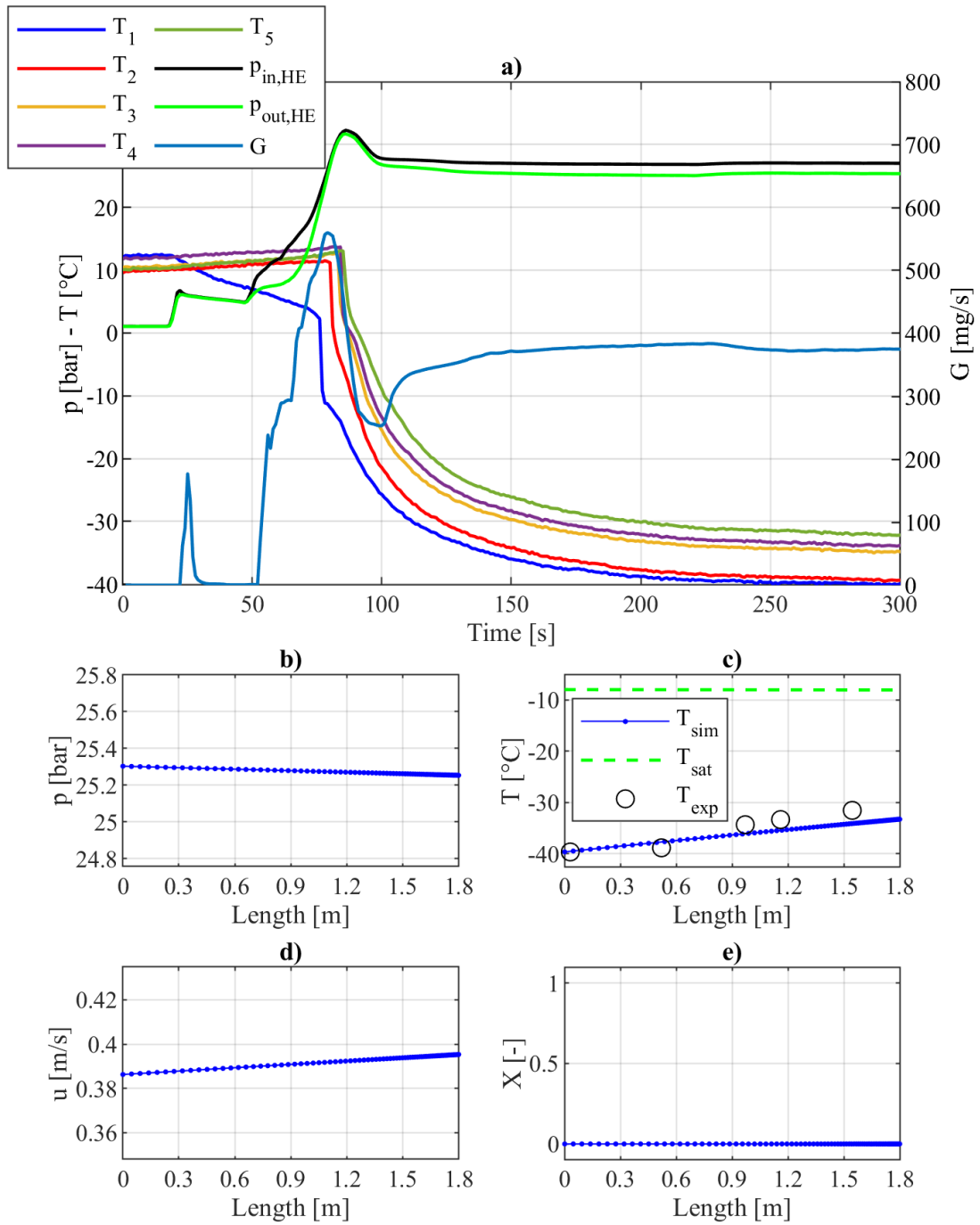


Figure 8.4. **a)**: Experimental $T_{cold}=-30$ °C. **[b-c-d-e)**: Capillary simulation with input value, experimental temperatures and mass flow rate obtained from **a)** averaging in the last 100s ($p_0=25.3$ bar, $T_0=-39.7$ °C and $G=377.0$ mg/s).

bench would be needed to instrument the return line and measure the pressure at intermediate points in the capillary as well. But it allows us to estimate the flow rates that can be disposed of under different supply conditions, and to calculate in advance the trends in fluid properties, making it possible to study the performance of a real probe.

Characteristic events

During the various recordings, unforeseen phenomena were encountered, there were two: an oscillatory phenomenon and a probably orifice blockage.

The first event can be observed in the trends shown in graph a) in Figure 8.5.

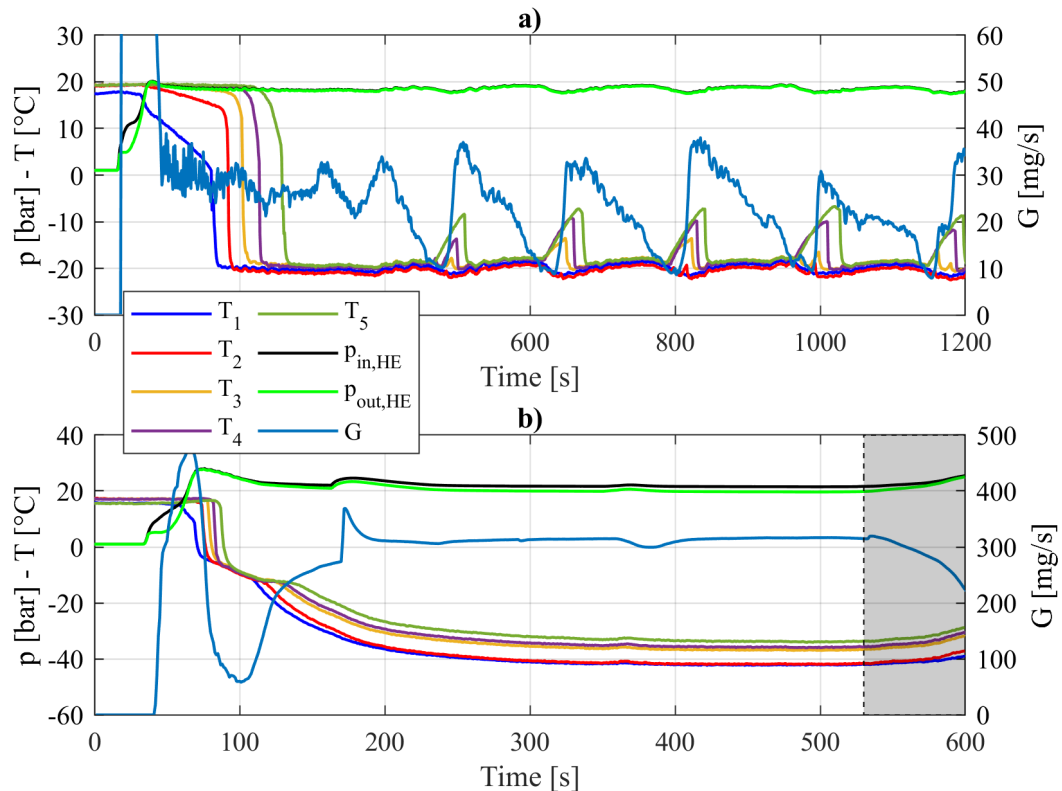


Figure 8.5. (High) Trend of measurements taken during the oscillatory phenomenon. (Low) Trend of measurements taken during the hole-clogging phenomenon.

Observing the temperature trends, it can be seen that around 200 s, in order of position they reach a temperature of around -20°C . After 400 seconds T_3 - T_4 - T_5 assume an oscillatory trend. At the same time, the mass flow rate shows a similar trend.

In fact, it seems as if the flow rate suddenly increases and then slowly decreases. If pressure trends are looked at closely, the same oscillatory pattern as previously mentioned can be seen.

This event could be due to flow metastability phenomena, which lead to the sudden condensation and vaporisation of the fluid. Probably inside the capillary due to the temperatures approaching saturation condition, slowly a bubble is created which reduces the flow rate and causes the temperatures to locally rise. Suddenly the bubble is disposed of, the flow rate rises quickly and as a result sub-cooled fluid flows again, with the temperature falling back to around -20°C .

It should also be noted that this oscillatory phenomenon has its own characteristic frequency with a period of 200s. It would be interesting to investigate this behaviour further.

An example of the second phenomenon is shown in graph **b)** Figure 8.5. Starting with the pressure measurements, it can be seen that after an initial peak before 100s, where the two curves seem to overlap, they begin to deviate, reaching "stationarity". On the other hand, observing the flow rate, as already noted in previous cases, the absence of pressure drop inside the exchanger coincides with the sudden decrease in mass flow rate. Then as the difference between the two pressures increases, so does the flow rate, until "stationary" conditions are reached. Similarly, temperature measurements seem to coincide at around 100s, and decrease until "stationary" condition. The temperature measured by the 5 thermocouple at 100s is the saturation one. Consequently the behaviour described is caused by the condensation of the fluid. "Stationary" is in quotation marks because in the highlighted range (550÷600 s), something seems to be happening. The pressures rise and overlap again and as expected the measured flow rate drops dramatically. This could be due to one of the holes being blocked, which would lead to the same trends as described above for pressure and flow rate. To confirm this, the reduction of mass flow rate leads to an increase in measured temperatures, as well as during the measurement session.

Blockage could be caused by freezing of the fluid flowing through the orifice. Photo **A** in Figure 8.6 shows the expansion chamber of the test bench where liquid N_2O accumulate at ambient pressure and saturation temperature.

The chamber is connected to a vacuum pump in order to reduce the pressure. And as shown in Photo **B** by reducing the pressure slightly the liquid freezes. Similarly, the freezing could be due to the combination of the pressure drop and temperature reduction that brings the fluid into a solidification condition near the hole, which causes the fluid to solidify, blocking the orifice.



Figure 8.6. **A**: experimental expansion chamber filled with liquid N_2O at ambient pressure and saturation temperature. **B**:the liquid start to freeze for the effect of a sudden reduction of pressure due to the connection of a vacuum pump.

Chapter 9

Performances of a commercial probe

Finally, the model was used to simulate a real probe. The Artic Front family of catheters, manufactured by Medtronic, was taken as a reference point. The dimensions implemented for the simulations are: $L=3.5$ m, $d_{IL}=0.31$ mm, $s_{IL}=78$ μm , $d_{H,RL}=2.5$ mm, $d_{holes}=62$ μm , $N_{holes}=4$ and $C_d=0.61$, $d_B=28$ mm, $\epsilon=1.0$ μm , while the global heat transfer coefficient was assumed equal to $k_B=350$ $\text{W}/(\text{m}^2\text{K})$. For performance evaluation, once the geometry has been defined, the input conditions of the capillary are required, to be defined case by case.

In the operating procedure, two cases can be identified: inflation and ablation.

Inflation phase

Going deeper into this first phase, it consists of sending the fluid in a gas-only condition to inflate the balloon. Two different procedures have been supposed.

The first consists in the reduction of the supply pressure, in order to obtain in the capillary a gas state fluid, even though the temperature is that at the outlet of the pre-cooler. This procedure was suggested by the informations obtained in [45] about a different CB developed by Boston Scientific. To simulate this case, it was decided to use a temperature of $T_0=-25^\circ\text{C}$ in line with the ranged provided by [17] and an inlet pressure of $p_0=12$ bar decided only to ensure gas-only conditions along the capillary.

The second possible approach, was derived by observing the patent [47], it was noted the presence of a system to let the fluid bypass the pre-cooler. Consequently, as it does not enter the exchanger, the fluid will arrive at the capillary in a gaseous state at room temperature, in order to inflate the balloon. For this reason a temperature of $T_0=18^\circ\text{C}$ was used for the simulation, while for the pressure it was selected $p_0=34$ bar, as it must be lower than the saturation one ($p_{sat}|_{18^\circ\text{C}}=49$ bar).

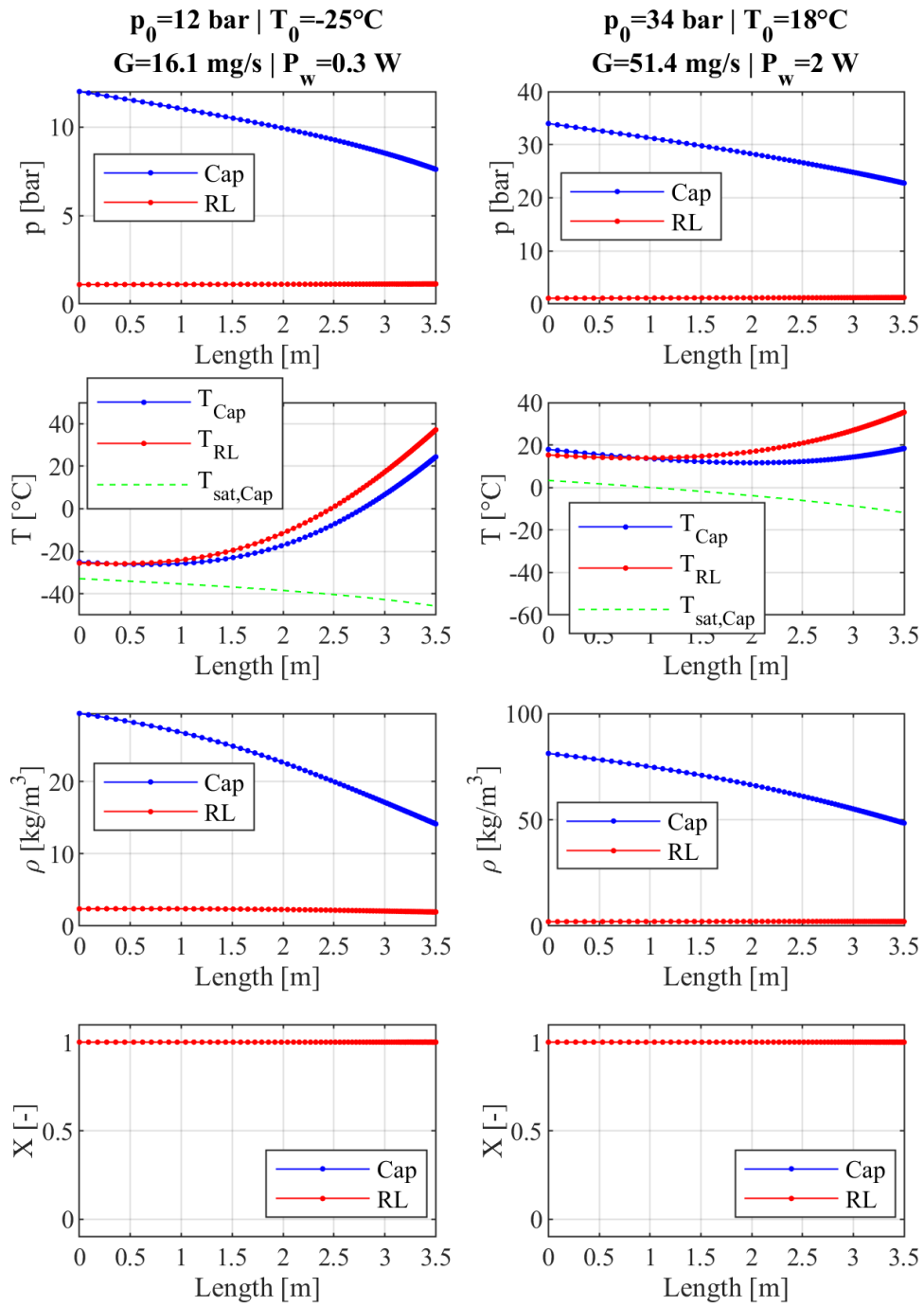


Figure 9.1. (left) Inflation phase obtained with inlet pressure reduction while keeping the subcooling ($T_0=-25^\circ\text{C}$ $p_0=12 \text{ bar}$). (right) Inflation phase with subcooling bypass ($p_0=34 \text{ bar}$ $T_0=18^\circ\text{C}$).

The two cases were simulated and the results are shown in Figure 9.1. The left column shows the trends for the first case while the right column the trends for the second case.

Starting from the temperature trends of the two cases, the values related to the capillary (T_{Cap}) always remain above the condensation temperature ($T_{sat,Cap}$), consequently the fluid is in gas state inside the capillary.

Moreover, having considered k_B equal to what has been calculated for the ablation conditions, in both cases, the fluid enters the return line with a temperature very close to the one imposed for the human body ($T_{body}=38^{\circ}\text{C}$). This implies that the balloon has exchanged heat completely with the tissue and that the return line inlet is at an higher temperature of the capillary outlet.

This leads to heating of the injection line, ensuring that despite expansion, the temperature is above the evaporation point.

This injection line heating effect brings the temperature reached at the end of the capillary close to 20°C in both cases, despite the different initial temperatures.

In the first case, due to the low mass flow rate ($G=16.1\text{ mg/s}$), return line totally influences the temperature of the injection line. In fact, for the capillary can be note an increasing trend, starting from the initial value of -25°C , the temperature increases by approximately 50°C .

While in the second case, for the higher flow rate ($G=51.4\text{ mg/s}$), the internal temperature of the capillary first decreases due to expansion, and then increases due to the return line effect. It is also curious to note that the temperature of the return line drops beyond that of the capillary due to the cooling caused by the continuous expansion of the fluid.

The different flow rates in the two cases are mainly due to the different inlet pressures.

Considering the temperatures reached inside the capillary, and the powers exchanged by the ball, $P_w=0.3\text{ W}$ for the first and $P_w=2\text{ W}$ for the second case, both solutions are possible. This is because in both cases the fluid reaches the expansion chamber in a gaseous state and at a temperature that prevents it from freezing in undesirable places, as also shown by the low power exchanged.

Ablation phase

Ablation is the main stage in using the probe. It consists of sending liquid N_2O through a capillary to make it expand in order to reduce the temperature of the fluid and absorb heat from the target. For operating conditions during the ablative phase, no precise data are provided. With regard to temperature, a Medtronic patent [47] gives the range $-20\div-30^{\circ}\text{C}$. The inlet pressure must be lower than the one inside the reservoir (around 49 bar). In line with these limitations, the initial

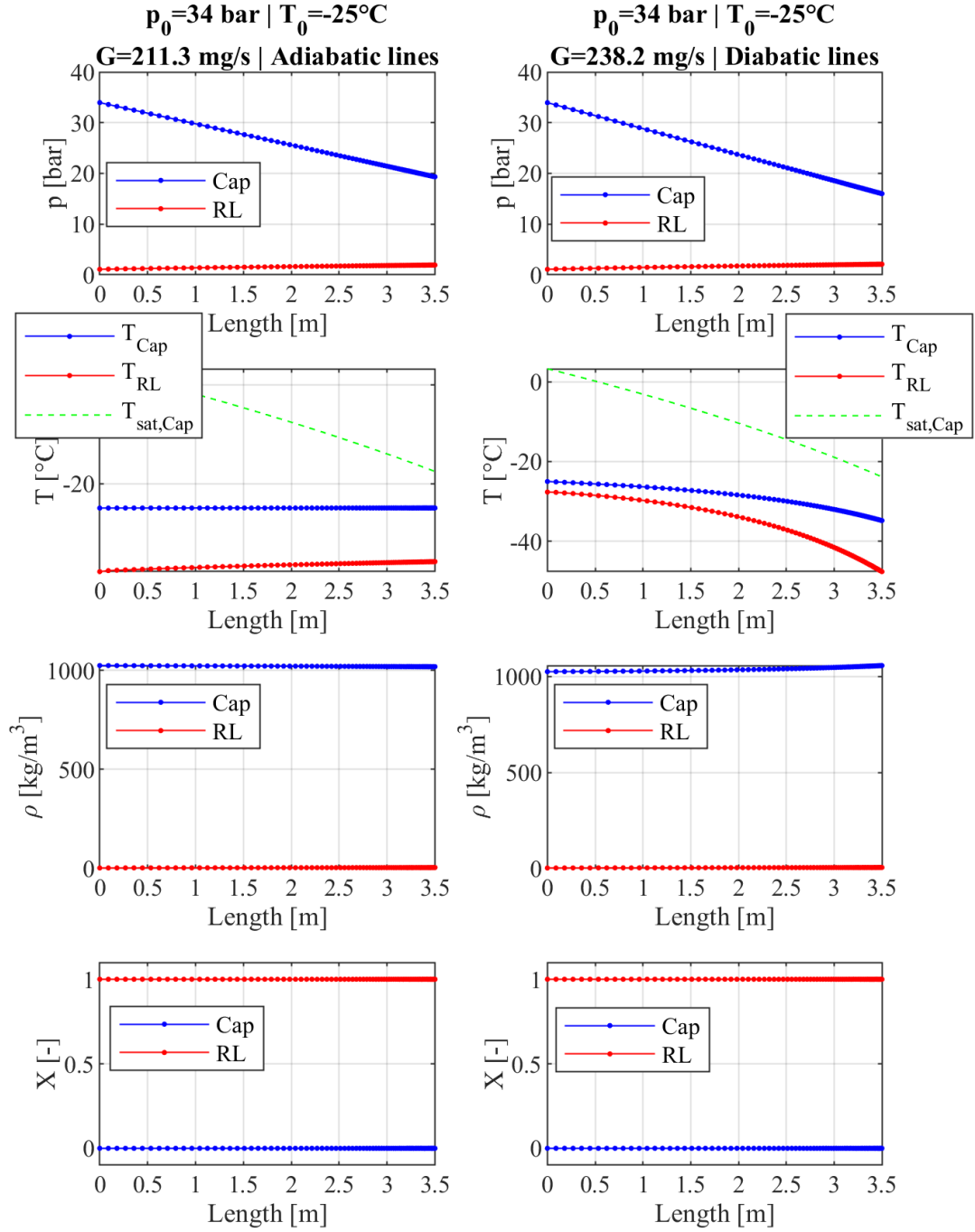


Figure 9.2. (left) Adiabatic case with $N_{\text{holes}}=4$ ($T_0=-25^\circ\text{C}$ $p_0=34$). (right) Diabatic case with $N_{\text{holes}}=4$ ($p_0=34 \text{ bar}$ $T_0=-25^\circ\text{C}$).

conditions are $p_0=34$ bar and $T_0=-25$ °C. Not knowing the real impact of the return line, the heat transfer between the two lines was either neglected or considered using heat transfer relations obtained from the literature but not experimentally validated for the case under consideration.

Defined the initial conditions, in Figure 9.2 the left column shows the solution with the adiabatic lines, while the right column shows the diabatic solution.

Starting with the temperature, it can be seen that in line with the values shown in the literature [43] the temperature of the balloon (T_B) corresponds to -36 °C and -47°C, respectively for the first and second case. This implies that in both cases the return line is at a lower temperature than the capillary. In the case without heat exchange, the two lines do not influence each other, the temperature of the return line only decreases due to expansion, while no notable variation can be observed in the capillary trend.

In the diabatic case, the two lines exchange heat with each other, and it can be seen that the return line has a regenerative effect, in fact this effect reduce the temperature of the capillary.

This cooling seems to directly influence the mass flow rate, in the first case $G=212$ mg/s while in the second $G= 238$ mg/s, both values are in line the range $200\div 230$ mg/s, obtained by a Medtronic patent [47].

Consequently, this regenerative effect of the return line, with the described inlet conditions and for $N_{holes}=4$ holes seems to increase the mass flow rate by 12 %.

N_f	G	$\frac{\Delta G}{G}$	T_B	p_B	P_W
4	212 mg/s	-	-36 °C	1.94 bar	64 W
5	221 mg/s	4.5 %	-39 °C	1.98 bar	66 W
6	227 mg/s	7.2 %	-41 °C	2.00 bar	68 W
7	231 mg/s	9.0 %	-42 °C	2.02 bar	69 W
8	234 mg/s	10.8 %	-43 °C	2.04 bar	70 W

Table 9.1. Effect of varying the number of holes (adiabatic lines) for inlet condition $T_0=-25$ °C $p_0=34$ bar (Ablation phase).

To observe the influence of the number of holes (N_{holes}), keeping the initial conditions equal to those of ablation ($p_0=34$ bar and $T_0=-25$ °C), the behaviour of both the case with and without regeneration was simulated by increasing from 4 to 8 the number of holes.

Looking at the two tables 9.1 for the adiabatic and 9.2 the diabatic. In both cases an increase of the number of holes leads to an increase in the flow rate. To note

N_f	G	$\frac{\Delta G}{G}$	T_B	p_B	P_W
4	238 mg/s	-	-47 °C	2.10 bar	74 W
5	255 mg/s	7.0 %	-53 °C	2.18 bar	79 W
6	266 mg/s	11.5 %	-57 °C	2.23 bar	82 W
7	273 mg/s	14.4 %	-60 °C	2.27 bar	84 W
8	277 mg/s	16.3 %	-61 °C	2.29 bar	86 W

Table 9.2. Effect of varying the number of holes (diabatic lines) for inlet condition $T_0=-25^\circ\text{C}$ $p_0=34$ bar (Ablation phase).

that doubling the flow area, does not imply the doubling of the mass flow rate. Increasing the number of hole from 4 to 8, so doubling the flow area, the increase in flow rate is 10.8% for the adiabatic case and 16.3% for the diabatic case, values in accordance with the 16% of increment stated in the [42] with the same increment in the number of holes.

As stated if the area of the orifices increases, the flow rate increases, but implies an increase in the pressure drop. This reduction of pressure upstream of the holes produces a reduction in the flow rate. The two effects affect each other, leading to an increase in flow rate that is lower than the increase in area.

Ball heat exchange effect

The balloon power heat exchanged was modelled by using a global heat transfer coefficient (k_B), with a suitable value to represent the effect. To determine it, it was imposed under the defined ablation conditions, a balloon temperature close to -40°C [36], obtaining $k_B=350 \text{ W}/(\text{m}^2\text{K})$.

Defined the value of k_B , two simulations were carried out under operative conditions ($p_0=34$ bar and $T_0=-25$ °C), one overestimating the heat transfer and one underestimating it.

Both cases could represent what happens when the probe is incorrectly positioned. An increase in the heat transfer coefficient could be due to blood flowing around the balloon. Under operating conditions, once the expansion chamber is positioned and inflated, blood flow is interrupted.

If the blood is able to flow, an higher heat exchange must be considered, which, considering only the forced convection of the blood [44], would imply higher exchanged powers with convective factor values of the order of $10^3 \div 10^4 \text{ W}/(\text{m}^2\text{K})$. While a reduction in the coefficient could be due to a positioning that prevents the

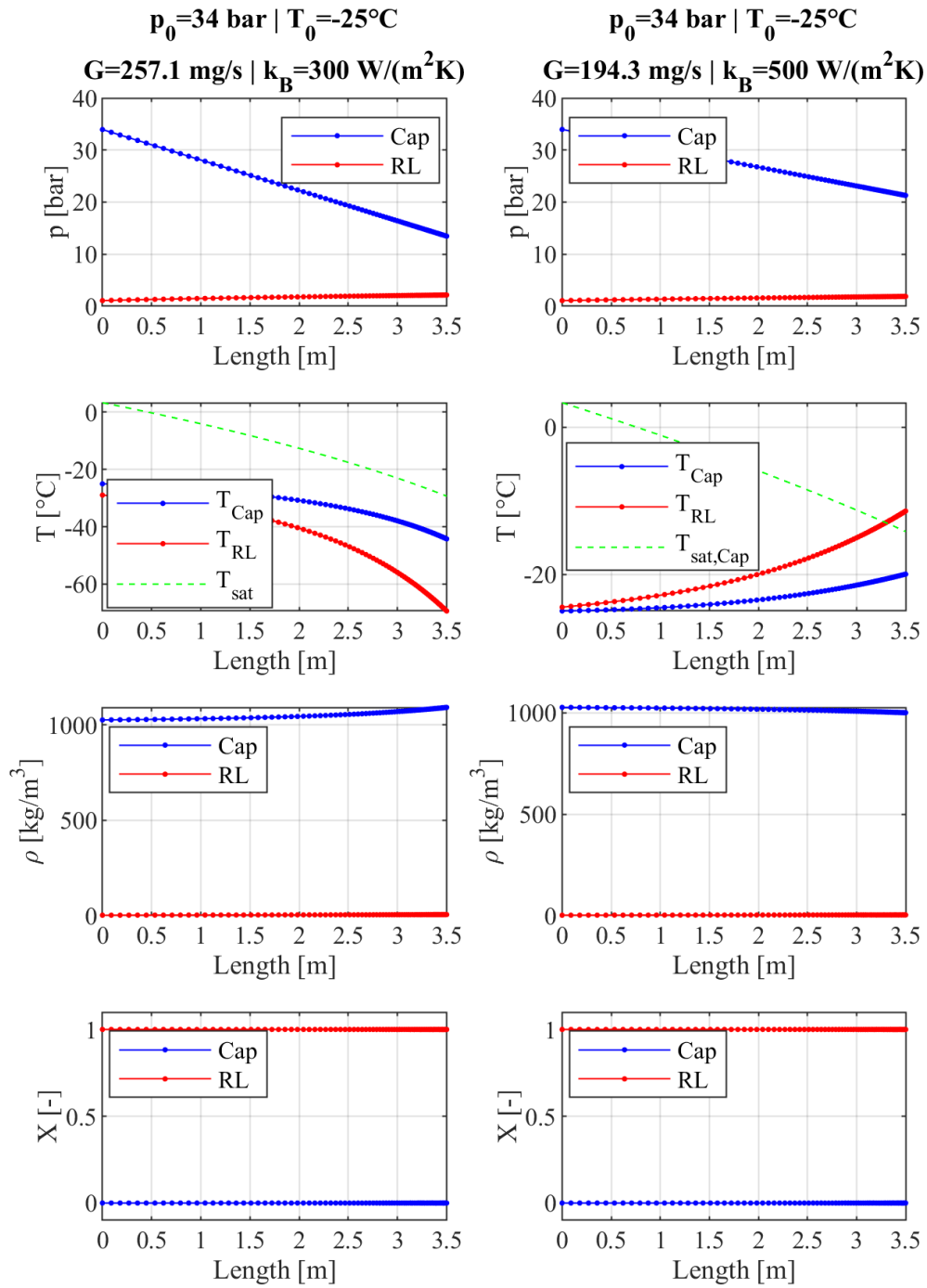


Figure 9.3. (left) Reduction in global heat exchange coefficient ($T_0=-25^\circ\text{C}$ $p_0=34$ bar $k_B=300$ W/(m²K)). (right) Increase in global heat exchange coefficient ($T_0=-25^\circ\text{C}$ $p_0=34$ bar $k_B=500$ W/(m²K)).

blood from flowing freely, but it is not optimal for the direction of the spray, which impacts on areas of the expansion chamber that are not in direct contact with the pulmonary vein.

Since it is not possible to predict the heat transfer coefficient in detail when the contact conditions vary, a 40% increase and a 15% reduction have been used to give an idea of what might happen, assuming $350 \text{ W}/(\text{m}^2\text{K})$ as the starting value.

Fig.9.3 shows the two cases just mentioned, the reduction in the heat exchanged represented by the left column and an increase in the right one.

Observing the temperature trends one can immediately see the difference in the return line.

An excessive exchange leads to a higher temperature in the expansion chamber and consequently inside the suction line. In this case, the temperature of the return line exceeds that of the capillary, this eliminates the regenerative effect, which in this case instead of further cooling the supply line, heats it, increasing the possibility of reaching saturation conditions, thus reducing the flow rate, considering that the calculated flow rate value corresponds to $G=194 \text{ mg/s}$, a reduction of 12% of the ablation case with 4 holes.

In the other case, the opposite effect can be seen, the reduction of the exchange leads to a greater regenerative effect than in the design case, leading to an increase in the disposable flow rate $G=257 \text{ mg/s}$, in this case resulting in an increase of 6%. This shows how important it is to have a detailed knowledge of the probe/tissue and capillary/return line heat exchange, because extremely different solutions can be obtained.

Chapter 10

Conclusions

In this thesis work, a numerical model was developed to simulate the fluid-dynamic and thermodynamic behaviour of a cryogenic fluid inside a cardiac balloon-based probe.

A homogeneous fluid model was used to simulate a two-phase fluid, thus considering the phases as one with intermediate properties.

A flow model through orifices was implemented in order to evaluate the flow rate in case of single and two-phase fluid, under critical and sub-critical conditions.

Empirical models of pressure drop and heat transfer were implemented based on the geometric and formation conditions of the second phase.

A preliminary evaluation of the friction models in the literature showed that the implemented relationships do not provide results with relevant differences, so the models of Cheng and Lin were chosen subjectively.

Using the modelling of a heat exchanger, a dimensioning and subsequent set-up of a test bench was carried out.

From the measurements taken, it was not possible to experimentally validate the whole model, but the ability to derive the disposed flow rate was checked, obtaining results in accordance with the experimental values, always with an error below 10%.

The simulated temperature trend under the experimental conditions approximates the experimental values.

The model results obtained by assuming different operating conditions were analysed. There is no precise information in the literature on the inlet conditions of the capillary at the different application stages. Ranges of values are given, making direct comparison impossible. Despite this, initial pressure and temperature values within the ranges provided have been chosen. The calculated flow rate values are consistent with those provided by the manual.

The effect of increasing the number of holes on the flow rate was analysed. Going from 4 to 8 holes, considering the regeneration, an increase of 16.3% was calculated,

in accordance with the claimed value, but considering the uncertainty of the feeding conditions, it a preliminary evaluation.

The influence of the regenerative effect between the return line and the capillary has on the mass flow rate was also analysed. Keeping the inlet conditions constant equal to the evaluated ablation ones, in the 4 holes case an increase in flow rate of 12% is obtained due to the influence of regeneration.

In order to evaluate the real performance of the model, and consequently its ability to calculate the evolution of the fluid, it would be necessary to improve the experimental setup by adding pressure transducers along the capillary, to evaluate the friction model and together with the temperature values, check the actual quality. While to validate the heat transfer models it would be necessary to instrument the return line, in order to evaluate the actual influence of the regenerative effect of the return line on the capillary.

The heat exchanged by the cryoballoon with the body tissue, currently evaluated by a fictitious equation using a global heat transfer coefficient, obtained by imposing temperature conditions inside the balloon, should be evaluated appropriately taking into account the impact effect of the spray on the inner surface of the balloon.

Bibliography

- [1] WW Akers. “Condensation inside horizontal tubes”. In: *Chem. Engg. Prog. Symp. Ser.* Vol. 56. 30. 1960, p. 145.
- [2] Thomas Arentz et al. “Clinical perspective”. In: *Circulation* 115.24 (2007), pp. 3057–3063.
- [3] P.K. Bansal and G. Wang. “Numerical analysis of choked refrigerant flow in adiabatic capillary tubes”. In: *Applied Thermal Engineering* 24.5 (2004), pp. 851–863. ISSN: 1359-4311. DOI: <https://doi.org/10.1016/j.applthermaleng.2003.10.010>.
- [4] Tadeusz Bohdal, Henryk Charun, and Małgorzata Sikora. “Comparative investigations of the condensation of R134a and R404A refrigerants in pipe minichannels”. In: *International Journal of Heat and Mass Transfer* 54.9 (2011), pp. 1963–1974. ISSN: 0017-9310. DOI: <https://doi.org/10.1016/j.ijheatmasstransfer.2011.01.005>.
- [5] Audrius Bredikis and David Wilber. *Cryoablation of Cardiac Arrhythmias E-Book*. Elsevier Health Sciences, 2011.
- [6] Hugh Calkins et al. “2017 HRS/EHRA/ECAS/APHRS/SOLAECE expert consensus statement on catheter and surgical ablation of atrial fibrillation: executive summary.” In: *J Interv Card Electrophysiol* 50.1 (2017), pp. 1–55.
- [7] J Camm et al. “Cryothermal mapping and cryoablation in the treatment of refractory cardiac arrhythmias.” In: *Circulation* 62.1 (1980), pp. 67–74.
- [8] Alberto Cavallini and Roberto Zecchin. “A dimensionless correlation for heat transfer in forced convection condensation”. In: *International Heat Transfer Conference Digital Library*. Begel House Inc. 1974.
- [9] Yi-He Chen et al. “Cryoablation vs. radiofrequency ablation for treatment of paroxysmal atrial fibrillation: a systematic review and meta-analysis”. In: *EP Europace* 19.5 (Jan. 2017), pp. 784–794. ISSN: 1099-5129. URL: <https://doi.org/10.1093/europace/euw330>.
- [10] Nian-Sheng Cheng. “Formulas for Friction Factor in Transitional Regimes”. In: *Journal of Hydraulic Engineering* 134.9 (2008), pp. 1357–1362. DOI: [10.1061/\(ASCE\)0733-9429\(2008\)134:9\(1357\)](https://doi.org/10.1061/(ASCE)0733-9429(2008)134:9(1357)).

- [11] Sukkarin Chingulpitak and Somchai Wongwises. “A comparison of flow characteristics of refrigerants flowing through adiabatic straight and helical capillary tubes”. In: *International Communications in Heat and Mass Transfer* 38.3 (2011), pp. 398–404. ISSN: 0735-1933. DOI: <https://doi.org/10.1016/j.icheatmasstransfer.2010.12.014>.
- [12] Mina K Chung et al. “Lifestyle and risk factor modification for reduction of atrial fibrillation: a scientific statement from the American Heart Association”. In: *Circulation* 141.16 (2020), e750–e772.
- [13] S.W. Churchill. “Friction-factor equation spans all fluid-flow regimes.” In: (1977).
- [14] A. Cicchitti et al. *Two-phase cooling experiments: pressure drop, heat transfer and burnout measurements*. Tech. rep. Centro Informazioni Studi Esperienze, Milan, 1959.
- [15] John G. Collier and John R. Thome. *Convective boiling and condensation*. Clarendon Press, 1994.
- [16] Irving S Cooper and Arnold St J Lee. “Cryostatic congelation: a system for producing a limited, controlled region of cooling or freezing of biologic tissues”. In: *The Journal of nervous and mental disease* 133.3 (1961), pp. 259–263.
- [17] *Data sheet, POLARx Cryoablation System*. URL: https://aiac.it/wp-content/uploads/2020/12/EP-639201-AA_POLARx-Brochure_A4_FINAL_IT_preview.pdf (visited on 07/06/2021).
- [18] F. D’Auria and P. Vigni. “Two-phase critical flow models”. In: (1980).
- [19] A.E. Dukler, M. Wicks III, and R.G. Cleveland. “Frictional pressure drop in two-phase flow: B. An approach through similarity analysis”. In: *AIChE Journal* 10.1 (1964), pp. 44–51. DOI: <https://doi.org/10.1002/aic.690100118>.
- [20] Hans K Fauske. *Contribution to the theory of two-phase, one-component critical flow*. Tech. rep. Argonne National Lab., Ill., 1962. DOI: [10.2172/4749073](https://doi.org/10.2172/4749073).
- [21] Andrew A Gage. “History of cryosurgery”. In: *Seminars in surgical oncology*. Vol. 14. 2. Wiley Online Library. 1998, pp. 99–109.
- [22] O. García-Valladares. “Numerical simulation and experimental validation of coiled adiabatic capillary tubes”. In: *Applied Thermal Engineering* 27.5 (2007), pp. 1062–1071. ISSN: 1359-4311. DOI: <https://doi.org/10.1016/j.applthermaleng.2006.07.034>.
- [23] Volker Gnielinski. “Heat Transfer Coefficients for Turbulent Flow in Concentric Annular Ducts”. In: *Heat Transfer Engineering* 30.6 (2009), pp. 431–436. DOI: <https://doi.org/10.1080/01457630802528661>.

- [24] S.E. Haaland. “Simple and Explicit Formulas for the Friction Factor in Turbulent Pipe Flow”. In: *Journal of Fluids Engineering* 105.1 (Mar. 1983), pp. 89–90. ISSN: 0098-2202. DOI: [10.1115/1.3240948](https://doi.org/10.1115/1.3240948).
- [25] Michel Haissaguerre et al. “Spontaneous initiation of atrial fibrillation by ectopic beats originating in the pulmonary veins”. In: *New England Journal of Medicine* 339.10 (1998), pp. 659–666.
- [26] GM Hass and CB Taylor. “A quantitative hypothermal method for production of local injury to tissue”. In: *Federation proceedings*. Vol. 6. 1. 1947, p. 393.
- [27] Christian J.L. Hermes, Cláudio Melo, and Joaquim M. Gonçalves. “Modeling of non-adiabatic capillary tube flows: A simplified approach and comprehensive experimental validation”. In: *International Journal of Refrigeration* 31.8 (2008), pp. 1358–1367. ISSN: 0140-7007. DOI: <https://doi.org/10.1016/j.ijrefrig.2008.04.002>.
- [28] Mohd Kaleem Khan, Ravi Kumar, and Pradeep K Sahoo. “An experimental study of the flow of R-134a inside an adiabatic spirally coiled capillary tube”. In: *international journal of refrigeration* 31.6 (2008), pp. 970–978.
- [29] Eric W Lemmon, Marcia L Huber, and Mark O McLinden. “NIST standard reference database 23: reference fluid thermodynamic and transport properties-REFPROP, version 8.0”. In: (2007).
- [30] Wei Li and Zan Wu. “A general criterion for evaporative heat transfer in micro/mini-channels”. In: *International Journal of Heat and Mass Transfer* 53.9 (2010), pp. 1967–1976. ISSN: 0017-9310. DOI: <https://doi.org/10.1016/j.ijheatmasstransfer.2009.12.059>.
- [31] S. Lin et al. “Local frictional pressure drop during vaporization of R-12 through capillary tubes”. In: *International Journal of Multiphase Flow* 17.1 (1991), pp. 95–102. ISSN: 0301-9322. DOI: [https://doi.org/10.1016/0301-9322\(91\)90072-B](https://doi.org/10.1016/0301-9322(91)90072-B).
- [32] H Martin et al. *VDI-Wärmeatlas*. Springer, 2002.
- [33] W.H. McAdams. “Vaporization inside horizontal tubes-II, Benzene oil mixtures”. In: *Trans. ASME* 64 (1942), pp. 193–200.
- [34] C Melo et al. “An experimental analysis of adiabatic capillary tubes”. In: *Applied thermal engineering* 19.6 (1999), pp. 669–684.
- [35] Samuel F.Yana Motta, José A.R Parise, and Sergio Leal Braga. “A visual study of R-404A/oil flow through adiabatic capillary tubes”. In: *International Journal of Refrigeration* 25.5 (2002), pp. 586–596. ISSN: 0140-7007. DOI: [https://doi.org/10.1016/S0140-7007\(01\)00057-3](https://doi.org/10.1016/S0140-7007(01)00057-3).

- [36] Robin Müssig and Johannes Hörth. “Cryoballoon model and simulation of catheter ablation for pulmonary vein isolation in atrial fibrillation”. In: *Current Directions in Biomedical Engineering* 4.1 (2018), pp. 473–475.
- [37] Matthew Olson et al. “Cardiac Ablation Technologies”. In: *Engineering in Medicine* (2019), pp. 83–118.
- [38] Chasik Park et al. “Experimentation and modeling of refrigerant flow through coiled capillary tubes”. In: *International Journal of Refrigeration* 30.7 (2007), pp. 1168–1175.
- [39] Vivek Y. Reddy et al. “The relationship between contact force and clinical outcome during radiofrequency catheter ablation of atrial fibrillation in the TOCCATA study”. In: *Heart Rhythm* 9.11 (2012), pp. 1789–1795. ISSN: 1547-5271. DOI: <https://doi.org/10.1016/j.hrthm.2012.07.016>.
- [40] S. Lin R.Y. Li and Z.H. Chen. “Numerical modeling of thermodynamic non-equilibrium flow of refrigerant through capillary tubes”. In: *ASHRAE Transactions* 96.1 (1990), pp. 542–549.
- [41] M. M. Shah. “Comprehensive correlations for heat transfer during condensation in conventional and mini/micro channels in all orientations”. In: *International Journal of Refrigeration* 67 (2016), pp. 22–41. ISSN: 0140-7007. DOI: <https://doi.org/10.1016/j.ijrefrig.2016.03.014>.
- [42] Florian Straube et al. “Differences of two cryoballoon generations: insights from the prospective multicentre, multinational FREEZE Cohort Substudy”. In: *Europace* 16.10 (2014), pp. 1434–1442.
- [43] Mitsuru Takami et al. “Impact of freezing time and balloon size on the thermodynamics and isolation efficacy during pulmonary vein isolation using the second generation cryoballoon”. In: *Circulation: Arrhythmia and Electrophysiology* 8.4 (2015), pp. 836–845.
- [44] Chanchana Tangwongsan. “Fluid velocity measurement using convective heat transfer coefficient measuring system”. In: *2007 IEEE/NIH Life Science Systems and Applications Workshop*. IEEE. 2007, pp. 81–84.
- [45] *Troubleshooting Guide, POLARx Cryoablation System*. URL: <https://www.bostonscientific.com/content/dam/bostonscientific/ep/portfolio-group/single-shot/in-depth/documents/EP-959203%20POLARx%20Cryoablation%20System%20Troubleshooting%20Guide.pdf> (visited on 07/06/2021).
- [46] Graham B Wallis. “Critical two-phase flow”. In: *International Journal of Multiphase Flow* 6.1-2 (1980), pp. 97–112.
- [47] Dan Wittenberger and Rachid Mahrouche. “Method and apparatus fo cryoadhesion”. U.S. pat. 9750555 B2. Sept. 5, 2017.

- [48] Fred HM Wittkamp et al. “Pulmonary vein ostium geometry: analysis by magnetic resonance angiography”. In: *Circulation* 107.1 (2003), pp. 21–23.
- [49] Tom Wong et al. “Clinical usefulness of cryomapping for ablation of tachycardias involving perinodal tissue”. In: *Journal of interventional cardiac electrophysiology* 10.2 (2004), pp. 153–158.
- [50] Massimo Zoni-Berisso et al. “Epidemiology of atrial fibrillation: European perspective”. In: *Clinical epidemiology* 6 (2014), p. 213.